# The ATP-exporting channel Pannexin-1 promotes CD8$^+$ T cell effector and memory responses

**Authors:** Trupti Vardam-Kaur[1,4,#], Alma Banuelos[1,#], Maria Gabaldon-Parish[1,5,#], Bruna Gois Macedo[1,#], Caio Loureiro Salgado[1], Kelsey Marie Wanhainen[2], Maggie Hanqi Zhou[1], Sarah van Dijk[1,6], Igor Santiago-Carvalho[1], Angad S. Beniwal[1,3], Chloe L. Leff[1], Changwei Peng[2,7], Nhan L. Tran[3], Stephen C. Jameson[2], Henrique Borges da Silva[1,3]*

**Affiliations:**

1 – Department of Immunology, Mayo Clinic Arizona, Scottsdale, Arizona, United States

2 – Center for Immunology, University of Minnesota, Minneapolis, Minnesota, United States

3 – Department of Cancer Biology, Mayo Clinic Arizona, Scottsdale, Arizona, United States

4 – Current address: Omeros Corporation, Seattle, Washington, United States

5 – Current address: University of New Mexico, Albuquerque, New Mexico, United States

6 – Current address: Biomedical Sciences Graduate Program, University of California, San Diego, California, United States

7 – Current address: Department of Immunology & HMS Center for Immune Imaging, Harvard Medical School, Boston, Massachusetts, United States

# – These authors contributed equally to this manuscript.

*Corresponding author and lead contact: BorgesdaSilva.Henrique@mayo.edu (H.BdS)

**Abstract**

Sensing of extracellular ATP (eATP) controls $CD8^+$ T cell function. Their accumulation can occur through export by specialized molecules, such as the release channel Pannexin-1 (Panx1). Whether Panx1 controls $CD8^+$ T cell immune responses *in vivo*, however, has not been previously addressed. Here, we report that T cell-specific Panx1 is needed for $CD8^+$ T cell responses to viral infections and cancer. We found that CD8-specific Panx1 promotes both effector and memory $CD8^+$ T cell responses. Panx1 favors initial effector $CD8^+$ T cell activation through extracellular ATP (eATP) export and subsequent P2RX4 activation, which helps promote full effector differentiation through extracellular lactate accumulation and its subsequent recycling. In contrast, Panx1 promotes memory $CD8^+$ T cell survival primarily through ATP export and subsequent P2RX7 engagement, leading to improved mitochondrial metabolism. In summary, Panx1-mediated eATP export regulates effector and memory $CD8^+$ T cells through distinct purinergic receptors and different metabolic and signaling pathways.

38 **Introduction**

39 Cytotoxic CD8$^+$ T cells control viral infections and solid tumors [1,2]. These cells, upon antigen
40 priming, quickly activate intracellular signaling pathways that lead to effector function and clonal
41 expansion [2]. The expansion and differentiation of effector CD8+ T cells are controlled by a
42 network of supporting cells and extracellular signals. Effector CD8$^+$ T cells differentiate into
43 either memory precursors (MP) cells or terminal effectors (TE), which perform distinct functions
44 and have different fates during T cell contraction. While MP cells become long-lived memory
45 CD8$^+$ T cell subsets, TE cells display heightened effector function and mostly die during
46 contraction [2], except for long-lived effector cells (LLECs) [3,4]. Effector CD8$^+$ T cells expansion
47 and differentiation are controlled by a network of supporting cells, and extracellular signals [2,5-7].
48 Various components of this network have been identified, including interactions with innate
49 immune cells[8,9] and cytokine sensing [10-13]. Extracellular accumulation of metabolites, however,
50 may also play an important role. Metabolites are often released as a byproduct of dead cells [14].
51 However, they can sometimes be actively released via transmembrane channels [15-17].
52 One of the most well-described metabolite transporters is the homo-heptameric release channel
53 Pannexin-1 (Panx1) [18,19]. Through release of “find-me” signals such as the nucleotide ATP,
54 Panx1 plays a critical role in the triggering of apoptotic cell clearance [19-22]. Panx1 can also
55 promote ATP export in healthy cells [20,23-27]. Panx1 is expressed by many immune and non-
56 immune cells, including T cells [28,29]. Panx-1-mediated ATP export promotes the anti-allergic
57 function of regulatory CD4$^+$ T cells (Tregs) [30]. Conventional CD4$^+$ T cells or CD8$^+$ T cells can
58 also export ATP via Panx1, influencing their function [28,31,32]. Panx1 also promote the export of
59 many other metabolites smaller than 1 kDa [19 20 21]. Metabolite export via Panx1, therefore, can
60 regulate T cell function and its downstream physiological consequences. However, no
61 comprehensive studies on the *in vivo* role of Panx1 in CD8$^+$ T cells have been done.
62 Extracellular ATP (eATP) is sensed by immune cells via purinergic receptors, like the high-
63 affinity ion channel P2RX4 or low-affinity ion channel P2RX7 [33]. We and others have previously

64 shown that P2RX7 is expressed by antigen-specific CD8$^+$ T cells [34-36] and is crucial for the
65 generation and survival of memory CD8$^+$ T cells [32,34,37]. In addition to Panx1 export, eATP can
66 accumulate through infection-induced tissue damage [38]. The role of P2RX7 for memory CD8$^+$ T
67 cell survival raises an interesting conundrum: these cells rely on consistent eATP signaling, yet
68 the release of ATP from tissue damage is likely absent after the pathogen is gone. In this work,
69 we investigated the role of Panx1 in the development of antigen-specific CD8$^+$ T cell responses
70 to viral infection. We found that Panx1 favors both the expansion of effector CD8$^+$ T cells and
71 the survival of memory CD8$^+$ T cells. Our data suggests that Panx1 promotes effector CD8$^+$ T
72 cells through a two-step process: following TCR priming, Panx1-mediated eATP export
73 promotes initial CD8$^+$ T cell activation in a P2RX4-dependent way. At a later stage, eATP is
74 insufficient to restore activation; Panx1-mediated activation leads to the accumulation of
75 extracellular lactate which is subsequently recycled into saturated phosphatidylinositol
76 biosynthesis. In contrast, memory CD8$^+$ T cells require Panx1 for survival through eATP export
77 and subsequent sensing of it via P2RX7. The overarching role of Panx1 for CD8$^+$ T cells is
78 evidenced by its importance in promoting optimal control of melanoma tumors by CD8$^+$ T cells,
79 as well as the induction of CD8$^+$ T cell-mediated graft-versus-host disease.
80
81
82 **Results**

83 **T cell-specific Panx1 promotes effector CD8$^+$ T cell accumulation**

84 We first sought to define how Panx1 affects CD8$^+$ T cell effector responses (gating strategy in
85 **Figure S1**). Panx1 mRNA levels are expressed by antigen-specific CD8$^+$ T cells (**Figure 1a,**
86 **Figure S2a**). These channels are functional in CD8$^+$ T cells, as ATP export was significantly
87 decreased – and intracellular ATP levels are concomitantly increased – when Panx1 is inhibited
88 by Trovafloxacin, an antibiotic with known Panx1-blocking function[22] (**Figure S2b**). Panx1 can
89 promote nucleotide export in apoptotic cells upon triggering by Caspase 3[22]. However, we did
90 not find increased To-Pro3 uptake in WT CD8$^+$ T cells in comparison to CD8$^+$ T cells deficient

91 for Panx1 (Panx1-KO) (**Figure S2c**), suggesting that Panx1 primarily drives metabolite export
92 from healthy CD8$^+$ T cells. Importantly, T cell-specific knockout of Panx1 does not affect CD8$^+$ T
93 cell thymic development (**Figure S2d**) or steady-state peripheral accumulation (**Figure S2e**).
94 Despite its presence in naïve CD8$^+$ T cells, Panx1 mRNA and protein expression levels are
95 increased in effector CD8$^+$ T cells (**Figures 1b-c, S2f-g**). Given its inhibitory role, we used
96 Trovafloxacin treatment of Lymphocytic Choriomeningitis Virus (LCMV)-infected mice
97 (previously transferred with LCMV gp33-TCR transgenic CD8$^+$ P14 cells) to test how Panx1
98 blockade affects the effector expansion of CD8$^+$ T cells. At one-week post-infection, we
99 observed significantly decreased numbers of splenic P14 cells (**Figure S3a**). Since multiple
100 other immune and non-immune cells can express Panx1 (**Figure S3b**), we used T cell-specific
101 KO systems to test the CD8$^+$ T cell-specific role of Panx1. LCMV-infected T cell-specific Panx1-
102 KO (CD4-Cre *Panx1*$^{fl/fl}$) mice had significantly decreased numbers of spleen effector gp33-
103 specific CD8$^+$ T cells (**Figure 1d**, left). Both KLRG1$^+$CD127$^-$ terminal effectors (TE) and
104 CD127$^+$KLRG1$^-$ memory precursors (MP) numbers were lower in CD4-Cre *Panx1*$^{fl/fl}$ mice
105 (**Figure 1d**, right). Similar results were found using alternative experimental systems: 1:1
106 WT:CD4-Cre *Panx1*$^{fl/fl}$ mixed bone marrow chimeras infected with LCMV (**Figures 1e-g**),
107 CRISPR-Cas9 deletion of Panx1 in P14 cells (sgPanx1; **Figures S4a-b**), and infection of WT
108 versus CD4-Cre *Panx1*$^{fl/fl}$ with influenza (**Figure S4c**) – despite no differences in the lung
109 accumulation of influenza-specific CD8$^+$ T cells being observed (**Figure S4d**).
110 We next measured which aspects of effector CD8$^+$ T cell function rely on Panx1 expression.
111 RNA-seq analysis of WT versus Panx1-KO CD8$^+$ T cells activated *in vitro* for 72h showed
112 decreased expression of many genes associated with the T cell receptor (TCR) signaling
113 pathway in Panx1-KO CD8$^+$ T cells (**Figure 1h**). Indeed, Panx1-KO CD8$^+$ T cells displayed
114 reduced proliferation *in vivo* (**Figures 1i-j**). In addition to proliferation defects, Panx1-KO CD8$^+$ T
115 cells from LCMV-infected mice expressed reduced levels of activation markers such as CD69 or
116 CD44 (**Figure 1k**). *In vitro* proliferative capacity (**Figures 1l-m**), expression of CD69, CD44 or

117 CD25 (**Figure 1m**) and production of IFN-γ (**Figure 1n**) by Panx1-KO CD8$^+$ T cells was also
118 impaired.
119 Panx1 acts as a release channel for metabolites such as eATP. Our data shows that Panx1-KO
120 affects effector CD8$^+$ T cell activation at a populational level, making it hard to distinguish
121 between paracrine versus autocrine roles for Panx1. To discern between these two possibilities,
122 we used 1:1 WT:Panx1-KO co-cultures of CD8$^+$ T cells in *in vitro* activation assays (**Figure**
123 **S4e**). As shown in **Figure S4f**, despite some paracrine rescue, the expression of CD69 and
124 proliferation of Panx1-KO CD8$^+$ T cells were still significantly lower than WT CD8$^+$ T cells, even
125 in 1:1 co-culture. These results, which agree with our 1:1 mixed bone marrow chimeras, suggest
126 a dominant autocrine role for Panx1 for effector CD8$^+$ T cells, despite some paracrine effects.
127 Panx1 is recruited to the immunological synapse after T cell priming [28]. Therefore, Panx1 may
128 promote the activation of CD8$^+$ T cells in a TCR-dependent manner. Indeed, upregulation of
129 TCR downstream signaling molecule Nur77 is significantly impaired in the presence of
130 Trovafloxacin (Panx1i) (**Figure 1o**). Additionally, no defects in early CD8$^+$ T cell activation were
131 observed in Panx1-KO CD8$^+$ T cells upon short-term stimulation with PMA and Ionomycin,
132 which bypass the TCR signaling pathway (**Figure 1p**), further indicating a TCR-dependent role
133 for Panx1. Finally, we measured if Panx1-KO would affect effector CD8$^+$ T cell survival. As
134 shown in **Figure 1q**, Panx1-KO effector CD8$^+$ T cells had increased percentages of FLICA$^+$ (PI$^+$)
135 apoptotic cells. Overall, our results show that Panx1 is necessary for the effector CD8$^+$ T cell
136 proliferation, activation, and resistance to apoptosis in response to acute viral infection.
137
138 **Panx1 regulates the intracellular metabolism of effector CD8$^+$ T cells**
139 Because the activation and effector differentiation of CD8$^+$ T cells require sequential metabolic
140 adaptations, we investigated how Panx1 controls the intracellular metabolism of CD8$^+$ T cells.
141 Naïve Panx1-KO CD8$^+$ T cells showed no defects in mitochondrial respiration, mitochondrial
142 mass, or membrane potential (**Figures 2a-b**). However, as early as 3h after stimulation and

143 following early defects in activation, Panx1 deficiency negatively affected mitochondrial mass
144 and membrane potential (**Figure 2c**, above), leading to sustained defects up to 72h post-
145 activation (**Figure 2c**, below). After 72h of activation, Panx1-KO CD8$^+$ T cells displayed reduced
146 engagement of bioenergetic pathways needed for initial CD8$^+$ T cell activation [39]: aerobic
147 glycolysis and mitochondrial respiration (**Figure 2d**). Similar defects in mitochondrial mass and
148 membrane potential were observed in Panx1-KO CD8$^+$ T cells at early time points *in vivo*
149 (**Figure S5a**).
150 Following initial activation, effector CD8$^+$ T cells must shift their metabolism towards preferential
151 usage of aerobic glycolysis for terminal effector differentiation[40]. *In vitro*-activated CD8$^+$ T cells
152 for 72h displayed profound defects in mRNA expression of genes associated with aerobic
153 glycolysis (**Figure 2e**). To understand how Panx1 regulates the metabolism of CD8$^+$ T cells at
154 this late activation stage, we used prolonged exposure of *in vitro*-activated CD8$^+$ T cells to IL-2,
155 mimicking effector-like conditions[41] (**Figure 2f**). Effector-like CD8$^+$ T cells exhibited reduced
156 engagement of aerobic glycolysis but showed no defects in mitochondrial respiration, mass, or
157 membrane potential (**Figures 2g-h**). To determine if Panx1 specifically affects the aerobic
158 glycolysis of late effector CD8$^+$ T cells, we sorted TE P14 cells from LCMV-infected mice (WT
159 versus T cell-Panx1-KO) for extracellular flux analyses. Panx1-KO TE cells showed reduced
160 glycolysis but normal mitochondrial respiration (**Figure 2i**). These results indicate that Panx1
161 plays a dominant role in promoting the metabolic adaptations required for initial CD8$^+$ T cell
162 activation (energetic metabolism increase) and effector CD8$^+$ T cell full differentiation (induction
163 of aerobic glycolysis).
164
165 **Panx1-KO defects in effector CD8$^+$ T cells can be rescued by exogenous eATP and**
166 **sodium lactate**
167 Both 72h-activated (**Figure S2b**) and IL-2-induced effector-like CD8$^+$ T cells (**Figure S5b**)
168 export ATP via Panx1. Due to this well-established role of Panx1 and previous evidence *in*

169 *vitro*[31,42] , we hypothesized that exogenous eATP could rescue the activation defects of Panx1-
170 KO CD8$^+$ T cells. Early (3h post-stimulation) activation defects are significantly restored: Nur77,
171 CD69, CD25 and CD44 upregulation in Panx1-KO CD8$^+$ T cells are all significantly restored by
172 eATP addition to cultures (**Figures 3a-b, S5c**). Consistent with a previous study[42], the eATP
173 rescue of Panx1-KO activation is abolished in the presence of 5-BDBD, a P2RX4 inhibitor
174 (**Figure S5c**). Indeed, P2RX4 deletion in CD8$^+$ T cells phenocopied the defects in effector CD8+
175 T cell expansion observed in Panx1 deficiency (**Figure S5d**). In contrast, P2RX7 deletion did
176 not affect the *in vitro* activation of CD8$^+$ T cells (**Figure S5e**).
177 In contrast, activation defects observed in Panx1-KO at 24h or later post-stimulation could not
178 be restored by exogenous eATP (**Figure 3c**). Exogenous eATP also failed to rescue Panx1-KO
179 defects in IL-2-induced effector-like CD8+ T cells (**Figure 3d**). These results suggest that other
180 metabolites may be needed to restore the activation of Panx1-deficient CD8$^+$ T cells. To
181 investigate further, we used untargeted metabolomics to identify the intracellular and
182 extracellular metabolites affected by Panx1-KO in effector-like and memory-like (IL-15-
183 stimulated; further details below) CD8$^+$ T cells (**Figure S5f-g**). We found >250 extracellular
184 metabolites with decreased levels in effector-like Panx1-KO supernatants, and >300 in memory-
185 like Panx1-KO supernatants (top 100 of each depicted in **Figure S5h**). Among the metabolites
186 decreased in Panx1-KO effector-like CD8$^+$ T cell supernatants, we found amino acids, fatty
187 acids, and metabolites from the glycolysis pathway (**Figure 3e**). One of these metabolites,
188 lactate, has recently been suggested to promote effector CD8$^+$ T cell activation [43,44, 45], despite
189 past contrary evidence [46]. The accumulation of extracellular lactate is likely to be a
190 consequence of decreased early activation in Panx1-KO CD8$^+$ T cells, as intracellular lactate
191 levels are also diminished (**Figure 3f**), and both intracellular and extracellular lactate levels in
192 WT versus Panx1-KO CD8$^+$ T cells are highly dependent on MCT1 and MCT4, the canonical
193 lactate transporters (**Figures 3f-g**); mRNA expression of MCT4 (*Slc16a3*), but not MCT1
194 (*Slc16a1*), was affected in Panx1-KO activated CD8$^+$ T cells (**Figure S5i**). Blockade of MCT1

195 and MCT4 significantly affected WT, but not Panx1-KO CD8$^+$ T cell proliferation and expression
196 of CD69 (**Figure 3h-i**), further suggesting that Panx1 promotes CD8$^+$ T cell activation through
197 indirect induction of extracellular lactate accumulation.
198 We then tested whether exogenous lactate would rescue the activation and proliferation of
199 Panx1-KO CD8$^+$ T cells. Sodium lactate (a pH-neutral lactate salt) significantly rescued Panx1-
200 KO CD8$^+$ T cell proliferation and activation (**Figure 3j**). Sodium lactate also significantly restored
201 the glycolysis and mitochondrial respiration of activated Panx1-KO CD8$^+$ T cells (**Figure 3k**).
202 The restoring effects of sodium lactate are abolished when the OXPHOS inhibitor Oligomycin is
203 concomitantly present (**Figure 3l**). Effector-like defects in CD69 expression and glycolysis were
204 restored by exogenous sodium lactate (**Figure 3m**). In contrast, early (3h post-stimulation)
205 activation defects of Panx1-KO could not be restored by sodium lactate (**Figure 3n**). Finally,
206 sodium lactate treatment significantly rescued the effector expansion of Panx1-KO P14 cells in
207 LCMV-infected mice (**Figure 3o, Fig. S6**). These findings indicate that Panx1 promotes the
208 early activation and full effector differentiation of CD8$^+$ T cells through export of eATP and
209 indirect control of lactate accumulation.
210

211 **Panx1 amplifies the consumption of carbon sources for full effector CD8$^+$ T cell**
212 **differentiation**

213 We found that Panx1-KO CD8$^+$ T cells have an overall defect in bioenergetic metabolism after
214 activation. Indeed, the accumulation of several TCA cycle metabolites is diminished in effector-
215 like CD8$^+$ T cells (**Figure 4a**). Because consumption of carbon sources is necessary for the
216 engagement of such pathways, we used carbon ($^{13}C$) tracing metabolomics to measure the
217 incorporation of glucose (**Figure 4b**) or lactate (**Figure 4c**). Compared to WT CD8$^+$ T cells,
218 Panx1-KO cells had decreased glucose incorporation of α-ketoglutarate, a rate-determining
219 intermediate of the TCA cycle fundamental for energetic metabolism[47]. In contrast, lactate
220 incorporation into citrate was decreased in Panx1-KO. Citrate, although a TCA cycle

221 intermediate, can be shuttled out of the mitochondria and serve as a substrate for fatty acid
222 synthesis[48], which is crucial for the full activation of effector CD8$^+$ T cells[49].
223 In screenings to identify additional metabolites (among the ones depicted in **Figure S5h**) that
224 rescue Panx1-KO CD8$^+$ T cell activation (**Figure S5j**), among the few other candidates found
225 was Hydroxylauric Acid, a medium-chain fatty acid [50]. Medium-chain fatty acids are used by
226 CD8$^+$ T cells for fatty acid biosynthesis. Intracellular phospholipid biosynthesis metabolites were
227 sharply decreased in Panx1-KO effector-like CD8$^+$ T cells (**Figure 4d**), including
228 phosphatidylinositol (PIs) (**Figures 4e, S5k**). PIs compose the immunological synapse [51], and
229 saturated (i.e., with less than 2 double bonds) phosphatidylinositol phosphates (PIPs) compose
230 lipid rafts found during late activation, to sustain effector function [49]. Panx1-KO effector-like
231 CD8$^+$ T cells had specific defects in saturated PIs (**Figures 4e, S5k**) and decreased lipid raft
232 formation as depicted by Cholera Toxin B (CTB) staining (**Figure 4f**) – which can be restored by
233 sodium lactate, in an MCT-1-dependent way (**Figure S5l**). Additionally, oleic acid, a PI
234 biosynthesis-forming medium-chain fatty acid [49], had decreased intracellular levels in Panx1-KO
235 CD8$^+$ T cells (**Figure S5m**) – possibly as a consequence from impaired initial activation and
236 engagement of bioenergetic metabolism. Exogenous oleic acid partially (but not completely)
237 restored Panx1-KO CD8$^+$ T cell activation (**Figure 4g**), suggesting that Panx1-mediated
238 accumulation of this fatty acid plays a role in effector CD8$^+$ T cell activation. The restoring
239 effects of sodium lactate for Panx1-KO CD8$^+$ T cell activation were abolished when an inhibitor
240 of CDIPT, the enzyme that catalyzes the biosynthesis of saturated fatty acids, is present
241 (**Figure 4h, S5n**). Saturated PI biosynthesis leads to activation of the MAP-kinase (MAPK)
242 signaling pathway to sustain CD8$^+$ T cell activation and effector function [49]. RNA expression of
243 several MAPK pathway genes is decreased in Panx1-KO effector-like CD8$^+$ T cells (**Figure 4i**),
244 and phosphorylated ERK1/2 levels are diminished in Panx1-KO CD8$^+$ T cells – which is restored
245 in the presence of sodium lactate (**Figure 4j**). Therefore, the Panx1-induced effects of sodium
246 lactate are associated with saturated PI generation and formation of lipid rafts.

247 Because of the Panx1 effects on glycolysis and the Panx1-dependent incorporation of glucose
248 into the TCA cycle, we investigated how Panx1-mediated activation could be dependent of
249 exogenous glucose. Glut1 expression is diminished in Panx1-KO *in vitro*-activated $CD8^+$ T cells,
250 which was restored by exogenous sodium lactate (**Figure 4k**). Exogenous glucose addition to *in*
251 *vitro* cultures led to minor, but statistically significant increases in IFN-γ production, glycolysis,
252 and mitochondrial respiration (**Figures 4l-m**). These results suggest that Panx1 promotes the
253 full effector differentiation of $CD8^+$ T cells through an increase in the consumption of carbon
254 sources.
255
256 **Panx1 is crucial for the survival of memory $CD8^+$ T cells**
257 Panx1 mRNA is also found in memory $CD8^+$ T cell subsets (**Figure 1a, S2a**). We also
258 investigated how Panx1 affects memory $CD8^+$ T cell establishment (gating strategies in **Figure**
259 **S1**). T cell-specific Panx1-KO resulted in significantly decreased numbers of circulating memory
260 (**Figure 5a**) and small intestine intraepithelial (SI-IEL) tissue-resident memory ($T_{RM}$; **Figure 5b**)
261 gp33-specific $CD8^+$ T cells. Similar defects were observed in 1:1 WT:Panx1-KO mixed bone
262 marrow chimeras, (**Figures 5c-d**). To test whether memory $CD8^+$ T cell survival is specifically
263 regulated by Panx1, we used a tamoxifen-inducible KO system (**Figure 5e**). Tamoxifen-induced
264 Panx1 ablation during the effector stage affected both the accumulation of effector $CD8^+$ T cells
265 and the establishment of memory $CD8^+$ T cells (**Figure S7**). Panx1-KO after memory
266 establishment resulted in a steady decline of $CD8^+$ T cell numbers (**Figure 5f**). The decrease in
267 memory $CD8^+$ T cell numbers with late Panx1 ablation was true for all subsets of circulating
268 memory, although the most pronounced decline was in central memory ($T_{CM}$) cells (**Figures 5g-**
269 **h**). Late Panx1-KO also led to a decrease in $T_{RM}$ cells, except for the SI-IEL compartment
270 (**Figure 5i**). These results highlight a crucial role for Panx1 specifically for the long-term survival
271 of memory $CD8^+$ T cells.
272

273
274 **Panx1 promotes memory CD8$^+$ T cell survival through the eATP receptor P2RX7 and the**
275 **AMPK metabolic pathway**

276 Panx1 is canonically described as an ATP exporter and has been linked with activation of the
277 eATP receptor P2RX7 [20,23-27],[32,52]. We had previously found a crucial role for P2RX7 in the
278 induction of memory CD8$^+$ T cells[32,34,37]. To test if Panx1 regulates memory CD8$^+$ T cells
279 through P2RX7, we used CRISPR-Cas9 [53] to induce Panx1-KO in WT and P2RX7-KO P14
280 cells, thus generating double-knockout (DKO) CD8$^+$ T cells (**Figure 6a**). Upon adoptive transfer
281 and LCMV infection, we observed similar P14 $T_{CM}$ cell numbers between Panx1-KO, P2RX7-KO
282 and DKO groups – all lower than WT P14 $T_{CM}$ cells (**Figure 6b**). These data suggest that Panx1
283 may regulate $T_{CM}$ cell establishment through P2RX7. LLEC P14 cell numbers were further
284 diminished in DKO cells if compared to either single-KO, suggesting a non-redundant role of
285 Panx1 and P2RX7 for this subset (**Figure 6b**, right). P2RX7 promotes memory CD8$^+$ T cell
286 differentiation through promotion of mitochondrial respiration[32]. Panx1-KO mirrored this
287 phenotype, with sorted MP cells displaying reduced mitochondrial respiration compared to WT
288 TE cells (**Figure 6c**). To better understand how Panx1 regulates the mitochondrial metabolism
289 of memory-phenotype CD8$^+$ T cells, we used prolonged IL-15 stimulation of *in vitro*-activated
290 cells to generate memory-like conditions[41] (**Figure 6d**). Panx1-KO memory-like CD8$^+$ T cells
291 displayed reduced mitochondrial respiration and no defects on glycolysis – leading to increased
292 ECAR/OCR ratios (**Figure 6e**). The Panx1-KO memory-like defects in mitochondrial respiration
293 and homeostasis were significantly restored by exogenous eATP, and this rescue effect was
294 blocked by the P2RX7 inhibitor A-438079 (**Figure 6f-g**). Panx1 also induced the extracellular
295 accumulation of lactate in memory-like CD8$^+$ T cells (**Figure S5g**), but sodium lactate could not
296 restore the mitochondrial defects of Panx1-KO memory-like CD8$^+$ T cells (**Figure 6h**). These
297 data suggest Panx1 promotes the mitochondrial fitness of memory-phenotype CD8$^+$ T cells
298 through induction of eATP accumulation and activation of P2RX7.

299 We have previously established that P2RX7 promotes memory CD8$^+$ T cells partly through
300 activation of the AMPK pathway [32]. AMPK can be triggered, among other signals, by increased
301 AMP-to-ATP ratios [54,55]. Since Panx1 blockade promoted increased intracellular ATP (**Figure**
302 **S2b**), we monitored activation of the AMPK pathway in Panx1-KO memory CD8$^+$ T cells. Panx1-
303 KO led to decreased phosphorylation of the downstream AMPK target Acetyl-CoA-Carboxylase
304 (pACC) in memory CD8$^+$ T cells, especially $T_{CM}$ cells (**Figure 6i**). In addition, Panx1-KO
305 memory-like CD8$^+$ T cells had reduced mRNA expression of several genes associated with the
306 AMPK pathway (**Figure 6j**). This suggests a connection between Panx1 promotion of memory
307 CD8$^+$ T cells and activation of the AMPK pathway. To test whether Panx1 promotes memory
308 CD8$^+$ T cells through AMPK, we co-transferred WT and Panx1-KO P14 cells into LCMV-infected
309 mice that were treated with AICAR, an AMPK pathway agonist. The Panx1-KO/WT P14 cell
310 ratios at the memory phase were significantly increased in AICAR-treated mice (**Figure 6k-l**),
311 suggesting a preferential rescue of Panx1-KO memory CD8$^+$ T cell generation by forced AMPK
312 activation. Moreover, Panx1-KO memory-like CD8$^+$ T cells cultured in the presence of AICAR
313 displayed increased mitochondrial function (**Figure 6m-n**). Our results indicate that Panx1
314 promotes the mitochondrial fitness and long-term establishment of memory CD8$^+$ T cells
315 through accumulation of eATP, induction of P2RX7 activation, and promotion of the AMPK
316 signaling pathway.
317
318

319 **Panx1 deficiency hinders tumor control or graft-versus-host disease induced by CD8$^+$ T**
320 **cells**

321 Given the importance of CD8$^+$ T cell responses in controlling solid tumors [56-58], we assessed the
322 role of Panx1 in CD8$^+$ T cell-mediated melanoma control. To circumvent any non-CD8+ T cell-
323 specific effects of Panx1, we used an adoptive cell therapy (ACT) model previously used by our
324 group[59,60]. *In vitro*-activated Panx1-KO P14 cells showed defects in limiting B16-gp33 tumor

325 growth and fail to promote survival of B16-gp33 tumor-bearing mice compared to activated WT
326 P14 cells (**Figures 7a-c**). We next evaluated the numbers and phenotype of adoptively
327 transferred WT and Panx1-KO P14 cells in tumor-bearing mice through co-transfer experiments.
328 We observed a significant underrepresentation of Panx1-KO P14 cells infiltrating B16 tumors,
329 with no differences detected in draining lymph nodes or spleen (**Figure 7d**). Among tumor-
330 infiltrating P14 cells, Panx1-KO cells exhibited increased signs of mitochondrial dysfunction
331 such as depolarized mitochondria, as well as decreased levels of mitochondrial mass or
332 membrane potential (**Figure 7e**). These data suggest that expression of Panx1 is important for
333 $CD8^+$ T cells to infiltrate tumors, maintain mitochondrial homeostasis, and perform optimal
334 antitumor function.
335 Finally, we tested the biological relevance of Panx1 for $CD8^+$ T cell disease-inducing responses
336 using an experimental model of graft-versus-host disease (GVHD). This model relies on the
337 adoptive transfer of naïve $CD8^+$ T cells from C57BL/6 mice into MHC-mismatched BALB/c
338 mice[61] (**Figure 7f**). Transfer of WT, but not CD4-Cre *Panx1*$^{fl/fl}$ $CD8^+$ T cells led to a precipitous
339 weight loss in recipient BALB/c mice (**Figure 7g**). These data indicate that Panx1 promotes
340 $CD8^+$ T cell responses that can cause deleterious effects, suggesting the potential utility of
341 Panx1 inhibition as a therapeutic target in these conditions.
342
343 **Discussion**
344 Sensing of extracellular metabolites promotes $CD8^+$ T cell metabolism, homeostasis, and
345 function [62-64]. The sources of these metabolites and how they affect $CD8^+$ T cell intracellular
346 pathways are still not fully understood. Our work suggests that, through the action of Panx1,
347 $CD8^+$ T cells utilize eATP for their own sensing, promoting $CD8^+$ T cell responses at the effector
348 and at the memory stage. Additionally, we found that Panx1, besides its well-known role as an
349 eATP exporter[20], can regulate $CD8^+$ T cell responses through indirect accumulation of
350 extracellular lactate. Both effector and memory-phenotype $CD8^+$ T cells induce eATP and

351 lactate extracellular accumulation via Panx1, ruling out differential metabolite export as a reason
352 why Panx1 controls effector and memory CD8$^+$ T cell establishment differently. Rather, the
353 outcome of the Panx1 role is dictated by the signaling pathways and specific requirements for
354 effector or memory CD8$^+$ T cells. In future studies, we will investigate whether this phenomenon
355 is generalizable for all metabolites exported via Panx1, or if certain molecules are exported
356 differentially in effector versus memory CD8$^+$ T cells.
357 We found a fundamental role of Panx1 in promoting effector CD8$^+$ T cell responses. Consistent
358 with previous reports, Panx1 controls the early activation of CD8$^+$ T cells through eATP export,
359 in a TCR priming and P2RX4-dependent way[42,65]. Unexpectedly, the role of Panx1 for the late
360 stages of CD8$^+$ T cell activation was not rescued by eATP. Instead, our data suggest that
361 Panx1-mediated accumulation of extracellular lactate, likely as a byproduct of early glycolytic
362 metabolism[66,67], promotes the complete effector CD8$^+$ T cell differentiation. While lactate has
363 been considered immunosuppressive due to its coupling with acidosis[46,68], lactate-induced
364 acidosis is primarily observed in hypoxic conditions, such as in the tumor microenvironment [69].
365 During T cell priming, lactate is present in a pH neutral condition, which is well-tolerated by cells
366 [70]. Our results indicate that Panx1-induced extracellular lactate can be recycled by CD8$^+$ T cells
367 via MCT-1, leading to saturated PI biosynthesis, lipid raft formation, induction of MAPK pathway
368 activation, and reinforcement of the effector CD8$^+$ T cell program. Our work provides additional
369 evidence that carbon sources induce the generation of optimal lipid raft structures for sustained
370 CD8$^+$ T cell activation [49]. Despite a minor role for glucose in our model, glucose-independent
371 sources such as lactate can be relevant carbon sources for CD8$^+$ T cell activation and effector
372 differentiation [43,44,66]. Panx1, therefore, may serve as a “link” between these two concepts by
373 indirectly inducing the accumulation of an extracellular lactate pool, which in turn is utilized by
374 activated CD8$^+$ T cells to sustain its effector differentiation.
375 Panx1 also promotes the survival of memory CD8$^+$ T cells. Our data suggest that Panx1 favors
376 the homeostasis of memory CD8$^+$ T cells through the export of eATP, which is, in turn, sensed

377 by P2RX7. These results are consistent with previous reports on *in vitro*-stimulated T cells [31,52]
378 and support our speculation that, during the memory phase, eATP levels are tightly regulated
379 around the pericellular space of memory $CD8^+$ T cells [32,71]. This process may seem, at first,
380 energetically futile: the export of ATP would lead to a decrease in intracellular levels and
381 subsequent lower availability for energy-demanding processes. However, there are potential
382 advantages to Panx1-induced eATP export. For example, it would ensure constant engagement
383 of P2RX7 to sustain $Ca^{2+}$ influx and subsequent mitochondrial health [72]. Indeed, Panx1-KO
384 memory-phenotype $CD8^+$ T cells display defective mitochondrial respiration. The exceptions
385 were $T_{RM}$ cells forming in tissues where potential alternative eATP sources are present: the SI-
386 IEL, where eATP can be microbiota-derived [37,73], and the influenza-infected lung, where release
387 of eATP by tissue damage may occur. Moreover, Panx1 export of ATP also impacts its
388 intracellular levels[32] and we have previously speculated the possible consequences of Panx1-
389 mediated intracellular ATP decrease for $CD8^+$ T cells [71]. Promotion of the AMPK pathway due to
390 decreased intracellular ATP in an LKB-dependent pathway favors memory $CD8^+$ T cell
391 homeostasis [74], which we have shown to rely on P2RX7 [32]. Here, we found that Panx1
392 promotes memory $CD8^+$ T cells through AMPK induction. Panx1-mediated intracellular
393 metabolite alterations could also have effects on lactate. Excess intracellular lactate can hinder
394 T cell activation [75], therefore Panx1-mediated lactate export can prevent this shutdown. We will
395 investigate this possibility in the future, which would suggest Panx1 also acts as a “metabolite
396 escape valve” for effector or memory $CD8^+$ T cells.
397 $CD8^+$ T cell-specific Panx1 also promotes melanoma control. At first, these results conflict with
398 human cancer data, which shows high *PANX1* gene expression linked with poor prognosis in
399 multiple tumors [76], including melanoma [77]. Our data, however, focus on the $CD8^+$ T cell-specific
400 roles of Panx1. Indeed, a recent report has shown that *PANX1* expression and $CD8^+$ T cell
401 abundance is linked to better prognosis against stage III colorectal cancer[78]. Our ACT
402 experiments suggest a model where Panx1 expression specifically in $CD8^+$ T cells promote

403 efficient tumor control. Because of the mitochondrial defects observed in intratumoral CD8$^+$ T
404 cells lacking Panx1, we speculate that, in the context of melanoma, the dominant role of Panx1
405 is to promote the longevity and homeostasis of tumor CD8$^+$ T cells. Additional studies will be
406 necessary to further understand this mechanism.
407 Here, we demonstrated that CD8$^+$ T cells need Panx1 channels for their proper activation,
408 expansion, and survival into memory phase. Beyond the classical nucleotide exporter role of
409 Panx1, our results unveiled an unexpected link between expression of Panx1 and extracellular
410 accumulation of lactate – which is necessary for the effector differentiation of CD8$^+$ T cells.
411 Defining how Panx1 acts as an amplifier of CD8$^+$ T cell responses will open new directions on
412 our understanding of how adaptive immune cells interact with their surrounding milieu in
413 response to disease. Our data suggests that, at least in part, CD8$^+$ T cells can use Panx1 to
414 generate a favorable extracellular microenvironment by recycling products of their own
415 intracellular metabolic pathways.
416

417 **Acknowledgments**

418 We thank the Borges da Silva and Lancaster labs (Mayo Clinic Arizona) for their intellectual
419 input. We are thankful to the animal facilities at Mayo Clinic Arizona and at the University of
420 Minnesota for technical assistance and mouse husbandry; T. Brehm-Gibson, C. Viso, I. Silva-
421 Junior and E. Martinez for cell sorting and Flow Cytometry Core Facility maintenance at Mayo
422 Clinic Arizona; and M. Petterson for technical assistance at the Mayo Clinic Rochester
423 Metabolomics Core. We thank K. Ravichandran (U-Virginia, now Washington University) for
424 providing the *Panx1*$^{fl/fl}$ mice. We thank G. Hasko (Rutgers University) and Matyas Sandor (U-
425 Wisconsin) for providing the *P2rx7*$^{fl/fl}$ mice. BGI Americas provided bioinformatic support and
426 resources that helped achieve the results reported within this paper. This work was supported
427 by an individual predoctoral F30 fellowship from the National Institutes of Health (NIH)
428 (F30CA250321) to K.M.W.; NIH grants R01AI038903 and R01AI145147 to S.C.J.; Mayo Clinic

429 Center for Biomedical Discovery Pilot Grant-2021, and NIH grants K99/R00A139381 and
430 R01A170649 to H.BdS.
431

432 **Author contributions**

433 Conceptualization, T.V-K., H.BdS.; Methodology, T.V-K., H.BdS.; Formal Analysis, T.V-K., A.B.,
434 M.G-P., B.G.M., K.M.W., C.L.L., S.C.J. and H.BdS.; Investigation, T.V-K., A.B., M.G-P., B.G.M.,
435 C.L.S., K.M.W., M.H.Z., S.vD., I.S-C., A.S.B., C.L.L., C.P., and H.BdS.; Resources, N.L.T.,
436 S.C.J. and H.BdS.; Data Curation, T.V-K., A.B., M.G-P., B.G.M. and H.BdS.; Writing – Original
437 Draft, T.V-K. and H.BdS.; Writing – Review & Editing, T.V-K., A.B., M.G-P., B.G.M., C.L.S.,
438 K.M.W., S.C.J, and H.BdS.; Supervision, H.BdS.; Project Administration, H.BdS.; Funding
439 Acquisition, S.C.J. and H.BdS.
440

441 **Declaration of interests**

442 H.BdS. and N.L.T. are advisors for International Genomics Consortium. The remaining authors
443 have no financial disclosures. The authors declare no competing interests.
444

445 **Inclusion and Diversity**

446 One or more of the authors of this paper self-identifies as an underrepresented ethnic minority
447 in their field of research or within their geographical location. One or more of the authors of this
448 paper self-identifies as a member of the LGBTQIA+ community.
449

450 **Figure Legends**

451 **Figure 1. CD8$^+$ T cell-specific Panx1 is required for T cell activation and effector**
452 **differentiation.** (**a**) *Panx1* mRNA expression from RNA-seq samples in the indicated subsets of
453 LCMV-gp33 transgenic P14 CD8$^+$ T cells. (**b**) Single-cell RNA-seq (scRNAseq) analysis of
454 effector P14 cells showing UMAP cluster distribution (left) and expression of *Panx1* mRNA in
455 each cluster (right). (**c**) Western Blot analysis of Panx1 expression in WT (CD4-Cre) or Panx1-
456 KO (CD4-Cre *Panx1*$^{fl/fl}$) CD8$^+$ T cells at 0h or 72h after activation with anti-CD3/CD28 + IL-2. (**d**)
457 WT (CD4-Cre) or CD4-Cre *Panx1*$^{fl/fl}$ mice were infected with LCMV-Arm. Numbers of total (left)
458 and TE, MP (right) spleen gp33$^+$ CD8$^+$ T cells at day 7 post-infection are shown. (**e-g**) A 1:1 mix
459 of bone marrow cells from CD4-Cre (WT; CD45.1$^+$) and CD4-Cre *Panx1*$^{fl/fl}$ (Panx1-KO; CD45.2$^+$)
460 mice was transferred into lethally irradiated C57BL/6 mice (CD45.1/2$^+$). After two months, BM
461 chimeric mice were infected with LCMV-Arm. The red dotted lines show the Panx1-KO:WT
462 ratios after two months of reconstitution. (**e**) Graphical scheme. (**f**) Representative flow
463 cytometry plots showing WT and Panx1-KO total, TE and MP spleen gp33$^+$ CD8$^+$ T cells at day
464 7 post-infection. (**g**) Panx1-KO/WT ratios of total (left) and of naïve, TE and MP spleen gp33$^+$
465 CD8$^+$ T cells (right) at day 7 post-infection. (**h**) Heatmaps showing the expression of TCR
466 signaling pathway genes from RNA-seq data of activated WT and Panx1-KO CD8$^+$ T cells. (**i**)
467 CD4-Cre or CD4-Cre *Panx1*$^{fl/fl}$ mice were infected with LCMV-Arm and evaluated at 3 days after
468 infection. Representative histograms (left) and average percentages (right) of Ki-67$^+$ gp33$^+$
469 CD8$^+$ T cells are shown. (**j-k**) CD4-Cre (WT; CD45.1/2$^+$) and CD4-Cre *Panx1*$^{fl/fl}$ (Panx1-KO;
470 CD45.2$^+$) P14 cells were labeled with Cell Trace Violet and co-transferred into LCMV-infected
471 recipient C57BL/6 (CD45.1$^+$) mice. (**j**) Histograms showing Cell Trace Violet dilution (left) and
472 graphs showing average gMFI values (right) are shown. (**k**) Representative flow cytometry plots
473 showing expression of CD44 and CD69 are shown in the left. In the right, average percentages
474 of CD44$^+$CD69$^+$ cells (above) and of CD62L$^+$ cells (below) are shown. (**l-q**) WT (CD4-Cre) or

475 Panx1-KO (CD4-Cre *Panx1*$^{fl/fl}$) CD8$^+$ T cells were activated *in vitro* (anti-CD3/CD28 + IL-2, and
476 in some cases PMA/Ionomycin) for up to 72h. In some experiments (**o**), WT Nur77-GFP CD8$^+$ T
477 cells were activated in the presence of vehicle (PBS; Control) or Trovafloxacin (Panx1 inhibitor;
478 Panx1i). (**l**) Representative flow cytometry plots showing expression of CD69 and dilution of Cell
479 Trace Violet at 24h, 48h and 72h after activation. (**m**) Percentages of Cell Trace Violet (CTV)
480 divided cells (top left), average gMFI values for CD44 (top right), and percentages of CD69$^+$
481 (bottom left) and CD25$^+$ (bottom right) cells at 24h, 48h and 72h after activation. (**n**)
482 Representative histograms showing expression of IFNγ (top) and average percentages of IFNγ$^+$
483 CD8$^+$ T cells (bottom) at 72h after activation. (**o**) Representative histograms showing Nur77-
484 GFP expression in control of Panx1i-treated cells (above), and average percentages of Nur77-
485 GFP$^+$ CD8$^+$ T cells (below) at 3h after activation are shown. (**p**) Average percentages of CD44$^+$
486 (left) and CD69$^+$ (right) cells at 3h after activation with either anti-CD3/CD28 or PMA/Ionomycin
487 are shown. (**q**) CD4-Cre and CD4-Cre *Panx1*$^{fl/fl}$ mice were infected with LCMV-Arm; at day 7
488 after infection, the percentages of FMK/FLICA$^+$ and PI$^+$ cells were assessed in gp33$^+$ CD8$^+$ T
489 cells. In the left, representative flow cytometry plots are shown; in the right, average
490 percentages of FMK/FLICA+ cells are depicted. (**c**) Data representative of 2 independent
491 experiments, n=4-5 per group. (**d-j, q**) Data from 2-3 independent experiments, n=5-12 per
492 experimental group. (**k**) Each replicate is a pool of activated CD8$^+$ T cells from three mice; n=3
493 replicates per experimental group. (**l-p**) Data from four independent experiments, n=7-11 per
494 experimental group per time point. ns – not significant ($p>0.05$), *$p<0.05$, **$p<0.01$, ***$p<0.001$,
495 ****$p<0.0001$, Unpaired t-test (**d, j-k, n-o**), One-way ANOVA with Tukey's post-test (**d, g, i, k, p-**
496 **q**), Two-way ANOVA with Bonferroni's post-test (**g, m**).

497 **Figure 2. Panx1 controls the intracellular metabolism of effector CD8$^+$ T cells.** (**a-b**) Naïve
498 CD4-Cre and CD4-Cre *Panx1*$^{fl/fl}$ CD8$^+$ T cells were analyzed for mitochondrial function. (**a**)
499 Measurements of Oxygen Consumption Rate (OCR) levels after sequential addition of

500 Oligomycin, FCCP and Rotenone/Antimycin A (top right); average OCR values at Spare
501 Respiratory Capacity (bottom right, SRC; see methods) are shown. (**b**) Mitotracker Green (Mito
502 Green) and TMRE; representative histograms are shown above, while average gMFI values are
503 shown below. (**c-d**) CD4-Cre or CD4-Cre *Panx1*$^{fl/fl}$ CD8$^{+}$ T cells were activated *in vitro* (anti-
504 CD3/CD28 + IL-2) for up to 72h. (**c**) Mito Green and TMRE average gMFI levels at 3h (above)
505 and 72h (below) after activation are shown. (**d**) Measurements of Extracellular Acidification Rate
506 (ECAR) levels after addition of Oligomycin (top left); measurements of Oxygen Consumption
507 Rate (OCR) levels after sequential addition of Oligomycin, FCCP and Rotenone/Antimycin A
508 (top right); average ECAR values at baseline (bottom left), average OCR values at baseline
509 (bottom middle) and Spare Respiratory Capacity (bottom right, SRC; see methods) are shown.
510 (**e**) Heatmap showing expression of genes from the Glycolysis pathway in 72h-activated CD8$^{+}$ T
511 cells; expression in memory-like CD8$^{+}$ T cells (with additional IL-15 treatment – more on Figure
512 6) are shown in comparison. (**f-h**) CD4-Cre or CD4-Cre *Panx1*$^{fl/fl}$ CD8$^{+}$ T cells were activated *in*
513 *vitro* (anti-CD3/CD28 + IL-2) for 72h, then further polarized into effector-like cells with IL-2 for
514 additional 72h. (**f**) Experimental design. (**g**) Measurements of Extracellular Acidification Rate
515 (ECAR) levels from effector-like CD8$^{+}$ T cells after sequential addition of Glucose, Oligomycin
516 and 2-DG (top left); in the top right, kinetics of OCR values. On the bottom, average baseline
517 ECAR and OCR values, and the ratios between ECAR and OCR values from effector-like CD8$^{+}$
518 T cells are shown respectively. (**h**) Average Mito Green and TMRE gMFI values for effector-like
519 CD8$^{+}$ T cells. (**i**) CD4-Cre and CD4-Cre *Panx1*$^{fl/fl}$ P14 cells were transferred into C57BL/6 mice
520 infected with LCMV-Arm. At day 7 post-infection, TE P14 cells were sorted. ECAR and OCR
521 kinetics (top), ECAR values (bottom left), OCR values (bottom center) and ECAR/OCR ratios
522 (bottom right) from sorted TE gp33$^{+}$ CD8$^{+}$ T cells are shown. (**a-d, f-i**) Data from 2-3
523 independent experiments, n=4-21 per experimental group. (**e**) Data from 2-3 biological
524 replicates per experimental group (from n=5-8 mice per group). ns – not significant ($p>0.05$),
525 *$p<0.05$, **$p<0.01$, ***$p<0.001$, ****$p<0.0001$, Unpaired t-test (**a-d, f-i**).

526 **Figure 3. Panx1 controls the activation of effector CD8$^+$ T cells through export of eATP**
527 **and late extracellular lactate accumulation.** (**a**) WT Nur77-GFP CD8$^+$ T cells were activated
528 in the presence of PBS or Panx1i, with the addition of vehicle or eATP. Nur77-GFP
529 representative histograms (left) and average Nur77-GFP$^+$ percentages (right) are shown. (**b-c**)
530 CD4-Cre or CD4-Cre *Panx1*$^{fl/fl}$ CD8$^+$ T cells were activated *in vitro* (anti-CD3/CD28 + IL-2) for up
531 to 48h, with the addition of vehicle or eATP at either the beginning of cultures (**b**), or at 20h after
532 activation (**c**). (**b**) Average percentages of CD69$^+$ cells at 3h after activation. (**c**) Average
533 percentages of CD44$^+$ and CD69$^+$ cells at 24h after activation (left); average percentages of Cell
534 Tracer Violet$^-$ cells (CTV % divided) at 48h after activation (right). (**d**) CD4-Cre or CD4-Cre
535 *Panx1*$^{fl/fl}$ effector-like CD8$^+$ T cells (with prolonged exposure to IL-2) were incubated in the
536 presence or absence of eATP; average percentages of CD69$^+$ cells and of ECAR values are
537 shown. (**e**) WT (CD4-Cre) or Panx1-KO (CD4-Cre *Panx1*$^{fl/fl}$) effector-like and memory-like CD8$^+$
538 T cell cultures were harvested, and intracellular lysates and supernatants were submitted for
539 untargeted metabolomics (GC-MS) analysis. Enrichment analysis showing pathways
540 preferentially represented in the metabolites from the supernatants of WT effector-like CD8$^+$ T
541 cells (WT>Panx1-KO). Levels (arbitrary units – AU) of l-lactate in the supernatants (left) and
542 intracellular lysates (right) of effector-like WT and Panx1-KO CD8$^+$ T cells are shown below. (**f-**
543 **g**) CD4-Cre or CD4-Cre *Panx1*$^{fl/fl}$ CD8$^+$ T cells were activated *in vitro* (anti-CD3/CD28 + IL-2) for
544 72h, and l-lactate measurements (mM) were done. (**f**) Intracellular lactate levels. (**g**)
545 Extracellular lactate levels, in the presence or absence of inhibitors for MCT1 (SR13800) and
546 MCT4 (VB124). (**h**) Average percentages of IFNγ$^+$ CD8$^+$ T cells at 72h after activation, with
547 addition of sodium lactate +/- MCT1i. (**i**) Representative histograms (left), and average
548 percentages of CTV % divided and CD69$^+$ cells at 48h after activation, with addition of vehicle,
549 MCT1i, MCT4i or MCT1/MCT4i. (**g-k**) CD4-Cre or CD4-Cre *Panx1*$^{fl/fl}$ CD8$^+$ T cells were
550 activated *in vitro* (anti-CD3/CD28 + IL-2) for up to 72h, in the presence of the indicated
551 metabolites or inhibitors. (**j**) Average percentages of CD44$^+$ and CD69$^+$ cells after 24h of

552 activation (left), and of CTV % divided cells at 48h after activation (right), with the addition of
553 vehicle or sodium lactate. (**k**) ECAR and OCR kinetics (left) and average baseline values (right)
554 at 72h after activation, with the addition of vehicle or sodium lactate. (**l**) Average percentages of
555 $CD69^+$ cells at 48h after activation, with addition or sodium lactate +/- oligomycin. (**m**) CD4-Cre
556 or CD4-Cre *Panx1*$^{fl/fl}$ effector-like $CD8^+$ T cells were incubated in the presence or absence of
557 sodium lactate (right); average percentages of $CD69^+$ cells and of ECAR values are shown. (**n**)
558 WT Nur77-GFP $CD8^+$ T cells were activated in the presence of PBS or Panx1i, with the addition
559 of vehicle or sodium lactate; average percentages of Nur77-$GFP^+$ cells (left), $CD69^+$ cells
560 (center), or $CD44^+$ cells (right) are shown. (**o**) WT (CD4-Cre) or Panx1-KO (CD4-Cre *Panx1*$^{fl/fl}$)
561 P14 cells ($CD45.2^+$) were transferred into LCMV-infected WT $CD45.1^+$ mice. Some mice were
562 treated with sodium lactate between days 1-3 post-infection, and spleen P14 cells were
563 analyzed at day 7 post-infection. Flow cytometry plots showing expression of CD127 and
564 KLRG1 (left) and the average numbers of TE, MP and DN P14 cells per spleen (right) are
565 shown. (**a-d, f-o**) Data from 2-3 independent experiments, n=3-14 per experimental group. (**e**)
566 Data from 3 biological replicates per experimental group (from n=3 mice per group). ns – not
567 significant ($p>0.05$), *$p<0.05$, **$p<0.01$, ***$p<0.001$, ****$p<0.0001$, One-way ANOVA with Tukey's
568 post-test (**a-d, f-o**) Unpaired t-test (**e**), Two-way ANOVA with Bonferroni's post-test (**m**).

569 **Figure 4. Panx1 promotes carbon source uptake and leads to maintenance of lipid rafts**
570 **in activated $CD8^+$ T cells.** (**a**) Levels (arbitrary units – AU) of pyruvate, malate, aspartate, and
571 citrate in the intracellular lysates of effector-like WT (CD4-Cre) or Panx1-KO (CD4-Cre *Panx1*$^{fl/fl}$)
572 $CD8^+$ T cells from untargeted metabolomics are shown. (**b-c**) CD4-Cre and CD4-Cre *Panx1*$^{fl/fl}$
573 $CD8^+$ T cells were activated *in vitro* (anti-CD3/CD28 + IL-2) for 72h; in the last 12h, either $^{13}C$-
574 Glucose (**b**) or $^{13}C$-Lactate (**c**) were substituted into the cultures for metabolite carbon tracing.
575 (**b**) Percentages of $^{13}C$-Glucose incorporation into citrate, isocitrate, a-ketoglutarate, and
576 alanine. (**c**) Percentages of $^{13}C$-Lactate incorporation into citrate and isocitrate. (**d**) Top enriched

577 intracellular pathways in WT effector-like CD8$^+$ T cells (compared to Panx1-KO), depicted from
578 the untargeted metabolomics from (**a**). (**e**) Levels (AU) of total PIs in CD4-Cre versus CD4-Cre
579 *Panx1*$^{fl/fl}$ effector-like CD8$^+$ T cells; polyunsaturated (2 or more double bonds) or saturated (1 or
580 less double bonds) PIs are depicted in white and grey, respectively. In the right, levels (AU) of
581 PIP(34:1) in CD4-Cre versus CD4-Cre *Panx1*$^{fl/fl}$ effector-like CD8$^+$ T cells. (**f**) CD4-Cre and CD4-
582 Cre *Panx1*$^{fl/fl}$ CD8$^+$ T cells were activated *in vitro* (anti-CD3/CD28 + IL-2) in the presence or not
583 of Sodium Lactate. Representative histograms (left) and average gMFI values (right) for Cholera
584 Toxin B are shown. (**g**) CD4-Cre and CD4-Cre *Panx1*$^{fl/fl}$ CD8$^+$ T cells were activated *in vitro*
585 (anti-CD3/CD28 + IL-2) in the presence or not of BSA-conjugated Oleic Acid. Average
586 percentages of IFNγ$^+$ CD8$^+$ T cells are shown. (**h**) CD4-Cre and CD4-Cre *Panx1*$^{fl/fl}$ CD8$^+$ T cells
587 were activated *in vitro* (anti-CD3/CD28 + IL-2) in the presence or not of Sodium Lactate and/or
588 the CDIPT inhibitor Inostamycin (CDIPTi). Average percentages of IFNγ$^+$ CD8$^+$ T cells are
589 shown. (**i**) RNA expression levels (AU) of the indicated PLCγ-MAPK signaling pathway genes in
590 CD4-Cre and CD4-Cre *Panx1*$^{fl/fl}$ CD8$^+$ T cells after 72h of activation. (**j**) CD4-Cre and CD4-Cre
591 *Panx1*$^{fl/fl}$ CD8$^+$ T cells were activated *in vitro* (anti-CD3/CD28 + IL-2) in the presence or not of
592 Sodium Lactate. Representative histograms (left) and average gMFI values (right) for
593 phosphorylated ERK1/2 (pERK1/2) are shown. (**k**) CD4-Cre and CD4-Cre *Panx1*$^{fl/fl}$ CD8$^+$ T cells
594 were activated *in vitro* (anti-CD3/CD28 + IL-2) in the presence or not of Sodium Lactate.
595 Average gMFI values for Glut1 are shown. (**l-m**) CD4-Cre and CD4-Cre *Panx1*$^{fl/fl}$ CD8$^+$ T cells
596 were activated *in vitro* (anti-CD3/CD28 + IL-2) in the presence or not of additional Glucose. (**l**)
597 Average percentages of IFNγ$^+$ CD8$^+$ T cells are shown. (**m**) ECAR kinetics, OCR kinetics,
598 baseline ECAR and SRC OCR values are respectively shown. (**a-e, i**) Data from 2-3 biological
599 replicates per experimental group (from n=3 mice per group). (**f-h, j-m**) Data from 2-3
600 independent experiments, n=4-7 per experimental group. ns – not significant ($p>0.05$), *$p<0.05$,
601 **$p<0.01$, ***$p<0.001$, ****$p<0.0001$, Unpaired t-test (**a, e, i**), One-way ANOVA with Tukey's post-
602 test (**f-h, j-m**).

603 **Figure 5. Panx1 promotes the long-term establishment of memory CD8$^+$ T cells.** (**a-b**)
604 CD4-Cre or CD4-Cre *Panx1*$^{fl/fl}$ mice were infected with LCMV-Arm and gp33$^+$ CD8$^+$ T cells were
605 tracked over time. Numbers of total, $T_{CM}$ and LLEC spleen gp33$^+$ CD8$^+$ T cells at day 42 post-
606 infection are shown in (**a**), while the numbers of SI IEL gp33$^+$ CD8$^+$ T cells at day 42 post-
607 infection are shown in (**b**). (**c-d**) A 1:1 mix of bone marrow cells from CD4-Cre (WT; CD45.1$^+$)
608 and CD4-Cre *Panx1*$^{fl/fl}$ (Panx1-KO; CD45.2$^+$) mice was transferred into lethally irradiated
609 C57BL/6 mice (CD45.1/2$^+$). After two months, BM chimeric mice were infected with LCMV-Arm.
610 The red dotted lines show the Panx1-KO:WT ratios after two months of reconstitution. Panx1-
611 KO/WT ratios of $T_{CM}$ and LLEC gp33$^+$ spleen CD8$^+$ T cells over time post-infection are shown in
612 (**c**). In (**d**), the Panx1-KO/WT ratios of SI IEL, Salivary gland, and kidney $T_{RM}$ gp33$^+$ spleen CD8$^+$
613 T cells over time post-infection are shown. (**e-i**) Recipient C57BL/6 mice (CD45.1$^+$) were
614 adoptively transferred with a 1:1 mix of P14 ERT2-Cre LSL-YFP *Panx1*$^{+/+}$ (WT; CD45.1/2$^+$) and
615 P14 ERT2-Cre LSL-YFP *Panx1*$^{fl/fl}$ (CD45.2$^+$) cells, then infected with LCMV-Arm. Infected mice
616 were treated with vehicle or tamoxifen (Tx) at the indicated time intervals. (**e**) Experimental
617 design. (**f**) *Panx1*$^{fl/fl}$/*Panx1*$^{+/+}$ P14 cell ratios in the blood over time post-infection, in mice treated
618 with vehicle or Tx between days 28-35 (d28-35) post-infection. Treatment periods is indicated by
619 the blue shaded box. (**g**) Representative flow cytometry plots showing the distribution of spleen
620 $T_{CM}$, $T_{EM}$ and LLEC *Panx1*$^{+/+}$ and *Panx1*$^{fl/fl}$ P14 cells from mice treated with Tx d28-35 at 63d
621 post-infection. (**h**) *Panx1*$^{fl/fl}$/*Panx1*$^{+/+}$ ratios of spleen $T_{CM}$, $T_{EM}$ and LLEC P14 cells from mice
622 treated with vehicle or Tx d28-35, at 63d post-infection. (**i**) *Panx1*$^{fl/fl}$/*Panx1*$^{+/+}$ P14 cell ratios in
623 SG and SI IEL at day 63 post-infection, in mice treated with Tx between days 28-35. (**a-d, f-i**)
624 Data from 3 independent experiments, n=6-12 per time point per experimental group. ns – not
625 significant (p>0.05), *p<0.05, **p<0.01, ***p<0.001, ****p<0.0001, One-way ANOVA with Tukey's
626 post-test (**a, h-i**), Unpaired t-test (**b**), Two-way ANOVA with Bonferroni's post-test (**c-d, f**).

627 **Figure 6. Panx1 promotes memory CD8$^+$ T cell maintenance through eATP export and**
628 **activation of the AMPK pathway.** (**a-b**) WT (CD4-Cre) or P2RX7-KO (CD4-Cre *P2rx7*$^{fl/fl}$) P14
629 cells (CD45.2$^+$) were *in vitro* activated for 24h, then were electroporated with the Cas9 protein
630 combined with sgRNAs for *Cd4* (sg*Cd4*; control) or *Panx1* (sg*Panx1*; Panx1-KO). After 48h of
631 resting with IL-2, P14 cells were transferred into recipient mice (CD45.1$^+$) infected with LCMV-
632 Arm. (**a**) Experimental design. (**b**) Numbers of total spleen P14 cells (left), spleen $T_{CM}$ P14 cells
633 (middle) and spleen LLEC P14 cells (right) at day 42 post-infection. (**c**) CD4-Cre and CD4-Cre
634 *Panx1*$^{fl/fl}$ P14 cells were transferred into C57BL/6 mice infected with LCMV-Arm. At day 7 post-
635 infection, MP P14 cells were sorted. OCR kinetics (left), average baseline OCR values (middle)
636 and average SRC OCR values (right) are shown. (**d-h**) CD4-Cre or CD4-Cre *Panx1*$^{fl/fl}$ CD8$^+$ T
637 cells were activated *in vitro* (anti-CD3/CD28 + IL-2) for 72h, then further polarized into memory-
638 like cells with IL-15 for additional 72h. (**d**) Experimental design. (**e**) In the left, OCR kinetics for
639 both groups are shown. In the right, average baseline OCR values, average SRC OCR values,
640 and average ECAR/OCR ratios are shown. (**f**) OCR kinetics (left) and average baseline OCR
641 values (right) are shown for memory-like cells with additional treatment with eATP +/- A-438079.
642 (**g**) Average TMRE gMFI values for memory-like cells with additional treatment with eATP +/- A-
643 438079. (**h**) OCR kinetics (left) and average TMRE gMFI values for memory-like cells with
644 additional treatment with sodium lactate. (**i**) CD4-Cre or CD4-Cre *Panx1*$^{fl/fl}$ mice were infected
645 with LCMV-Arm and analyzed at 60 days post-infection. Histograms showing pACC staining
646 (top) and average pACC gMFI values (bottom) are shown for memory gp33$^+$ CD8$^+$ T cells. (**j**)
647 Heatmap showing expression of genes from the AMPK and FOXO1 pathways in memory-like
648 CD8$^+$ T cells; expression in CD8$^+$ T cells (with 72h post-activation) are shown in comparison. (**k-**
649 **l**) CD4-Cre (WT; CD45.1/2$^+$) or CD4-Cre *Panx1*$^{fl/fl}$ (Panx1-KO; CD45.2$^+$) P14 cells were
650 transferred into WT (CD45.1$^+$) mice infected with LCMV-Arm; between days 1-7 post-infection,
651 mice were treated with AICAR. (**k**) pACC expression in P14 cells. (**l**) Panx1-KO/WT P14 cell
652 ratios for spleen total (top) and $T_{CM}$ (bottom) cells are shown. (**m-n**) CD4-Cre or CD4-Cre

653 *Panx1*$^{fl/fl}$ CD8$^{+}$ T cells were activated *in vitro* (anti-CD3/CD28 + IL-2) then polarized into
654 memory-like cells, with additional treatment with vehicle or AICAR. (**m**) pACC expression in
655 CD8$^{+}$ T cells. (**n**) Average TMRE gMFI values (left), OCR kinetics (middle), and average
656 baseline OCR values (right) are shown. (**b-c, e-i, k-n**) Data from 2-3 independent experiments,
657 n=4-13. (**j**) Data from 2-3 biological replicates per experimental group (from n=5-8 mice per
658 group). ns – not significant (p>0.05), *p<0.05, **p<0.01, ***p<0.001, ****p<0.0001, One-way
659 ANOVA with Tukey's post-test (**b, f-i, m-n**), Unpaired t-test (**c, e, k-l**).

660 **Figure 7. Cell-specific Panx1 promotes antitumor CD8$^{+}$ T cell responses and graft-versus-**
661 **host disease *in vivo*.** (**a-e**) WT (CD4-Cre) and Panx1-KO (CD4-Cre *Panx1*$^{fl/fl}$) P14 cells were
662 activated *in vitro* (α-CD3, α-CD28, IL-2 and IL-12) for 72h. After this period, P14 cells were
663 transferred individually (**a-c**) or co-transferred (**d-e**) into B16.gp33 tumor-bearing mice. The
664 tumor sizes and survival of individually transferred mice were tracked over time post-tumor
665 inoculation; the numbers and phenotype of transferred P14 cells were assessed at 20 days
666 post-tumor inoculation in co-transferred mice. (**a**) Individual tumor growth values over time. (**b**)
667 Average tumor areas at day 14 post-tumor inoculation are shown. (**c**) Survival curves of
668 individually transferred mice over time. (**d**) Average Panx1-KO/WT P14 cell number ratios in the
669 indicated organs. (**e**) Average values for Mito Green (MTG) gMFI (left), TMRE gMFI (middle)
670 and percent of P14 cells with depolarized mitochondria (MTG$^{hi}$TMRE$^{-}$; right). (**f-g**) In other
671 experiments, BALB/c mice were lethally irradiated and reconstituted with either BALB/c BM cells
672 (No transfer), BM + spleen CD8$^{+}$ T cells from CD4-Cre mice (+ WT CD8) and BM + spleen
673 CD8$^{+}$ T cells from CD4-Cre *Panx1*$^{fl/fl}$ mice (+ Panx1-KO CD8). (**f**) Experimental design. (**g**)
674 Average survival values over time after cell transfer. (**a-g**) Data from 2-3 independent
675 experiments, n=5-20 per experimental group. ns – not significant (p>0.05), *p<0.05, **p<0.01,
676 ***p<0.001, Kaplan-Meier Survival curve analysis (**e**), Unpaired t-test (**g-f**), One-way ANOVA
677 with Tukey's post-test (**b**), Two-way ANOVA with Bonferroni's post-test (**g**).

678 **Materials and Methods**

679

680 **Lead contact**

681 Further information and requests for resources and reagents should be directed to and will be
682 fulfilled by the lead contact, Henrique Borges da Silva (borgesdasilva.henrique@mayo.edu).

683

684 **Materials availability**

685 No new unique reagents were generated in this study.

686

687 **Data and code availability**

688 • The data that support the findings of this study are available from the corresponding authors on
689 request.

690 • All sequencing reads generated in this study and processed RNA expression matrices are
691 deposited in NCBI's GEO and are publicly available as of the date of publication. The accession
692 numbers GSE217292 and GSE218643 are correspondent to the RNAseq analyses generated in
693 this paper.

694 • Any additional information required to reanalyze the data reported in this paper is available from
695 the lead contact upon request.

696

697 **Mice**

698 Male and female 6- to 8-week-old adult BALB/c, C57BL/6 (B6) and B6.SJL (expressing the
699 CD45.1 allele) mice were purchased from Jackson and Charles River and were allowed to
700 acclimate to our housing facilities for at least one week. CD4-Cre, Nur77-GFP, ERT2-Cre and
701 R26-EYFP (LSL-YFP) mice were obtained from Jackson Laboratories. *P2rx7*$^{fl/fl}$ mice were
702 obtained from Drs. Gyorgy Hasko (Rutgers University) and Matyas Sandor (U-Wisconsin).
703 *Panx1*$^{fl/fl}$ mice were obtained from Dr. Kodi Ravichandran (U-Virginia; now Washington

704 University). LCMV-$D^b$ GP33-specific TCR transgenic P14 mice were bred in-house at the
705 University of Minnesota and then transferred to Mayo Clinic Arizona. P14 mice were fully
706 backcrossed to B6, CD4-Cre *P2rx7*$^{fl/fl}$ and CD4-Cre *Panx1*$^{fl/fl}$ mice, with introduction of CD45.1
707 and CD45.2 congenic markers for identification. Animals were maintained under specific-
708 pathogen-free conditions at Mayo Clinic Arizona and at the University of Minnesota. In all
709 experiments, mice were randomly assigned to experimental groups. All experimental
710 procedures were approved by the institutional animal care and use committee at Mayo Clinic
711 Arizona (IACUC A00005542-20) and at the University of Minnesota (IACUC 1709-35136A).
712
713 **Viral strains**
714 LCMV (Armstrong strain) was maintained at −80°C until infection and diluted to $2x10^6$ PFU/ml in
715 PBS. Influenza (PR8 strain) was maintained at −80°C and diluted to $7x10^4$ PFU/ml in PBS at the
716 time of infection studies.
717
718 **Infection studies**
719 WT (CD4-Cre, ERT2-Cre-LSL-YFP), CD4-Cre *Panx1*$^{fl/fl}$, ERT2-Cre-LSL-YFP-*Panx1*$^{fl/fl}$, and
720 CD4-Cre *P2rx7*$^{fl/fl}$ P14 cells were adoptively transferred into naive wild-type mice, which were
721 infected with LCMV-Armstrong ($2 \times 10^5$ PFU, intraperitoneally (i.p.)). Sometimes, CD4-Cre or
722 CD4-Cre *Panx1*$^{fl/fl}$ mice were infected with LCMV Armstrong. In other experiments, CD4-Cre or
723 CD4-Cre *Panx1*$^{fl/fl}$ mice were infected with Influenza-PR8 (1400 PFU, intranasally (i.n.)). In
724 some experiments, LCMV-infected mice were treated with Trovafloxacin (4.2 mg x $kg^{-1}$ mouse,
725 Sigma-Aldrich) or Sodium Lactate (1.68 g x $kg^{-1}$ mouse, Sigma-Aldrich)[69] between days 1-7
726 after infection.
727
728 **Tumor inoculations**

729 WT or CMV-Cre *Panx1*$^{fl/fl}$ mice were injected subcutaneously with 1.5 x $10^5$ B16.F10 or 3 x $10^5$
730 B16.F10.gp33 cells in the right flank. In some experiments, after tumors became palpable (~7
731 days), tumor-bearing mice received 5 x $10^5$ activated CD4-Cre or CD4-Cre *Panx1*$^{fl/fl}$ P14 cells
732 (or 2.5 x $10^5$ of a 1:1 mix of these two P14 populations for co-transfer experiments). Tumor
733 growth was monitored by measuring height and width with calipers until mice reached an
734 endpoint criterion of 144 $mm^2$ or ulceration. When indicated in the figures, tumor-bearing mice
735 were sacrificed for flow cytometry analysis.
736
737 **Bone marrow chimeras**
738 CD45.1/2$^+$ WT mice were reconstituted with a 1:1 mixture of CD4-Cre (CD45.1$^+$) and CD4-Cre
739 *Panx1*$^{fl/fl}$ (Panx1-KO, CD45.2$^+$) following lethal irradiation (2 x 450 Rad). Two months following
740 irradiation, mice were infected with LCMV-Armstrong.
741
742 **GVHD mouse model**
743 GVHD mouse experiments were done as described previously (PMID: 11850710). BALB/c mice
744 were lethally irradiated (2 x 450 Rad) and reconstituted with either bone marrow cells from
745 BALB/c or C57BL/6 mice. In the mice transferred with C57BL/6 BM cells (1 x $10^7$ cells), spleen
746 CD8$^+$ T cells from either CD4-Cre or CD4-Cre *Panx1*$^{fl/fl}$ mice were transferred together (2 x $10^6$
747 cells). Weight loss was monitored in recipient BALB/c mice for 7 days.
748
749 **Administration of tamoxifen in mice**
750 Tamoxifen (Sigma-Aldrich, diluted in Sunflower Oil) was administered to mice i.p. at a daily dose
751 of 1 mg [37]. Two different treatment periods were used, in which Tamoxifen was given between
752 days 1-4 or between days 28-35 after LCMV-Armstrong infection.
753
754 **Primary cell cultures**

755 Total $CD8^+$ T cells or P14 cells were obtained from 6- to 8-week-old mice with a C57BL/6
756 background. Cells were cultured in complete RPMI media: RPMI 1640 (Corning) supplemented
757 with 10% Fetal Bovine Serum (Atlanta Biologicals), 100 U/ml penicillin/streptomycin (Thermo
758 Fisher Scientific) and 2 mM L-glutamine (Corning). All cells were cultured at 37°C in a
759 humidified atmosphere containing 5% $CO_2$.
760
761 ***In vitro* activation of $CD8^+$ T cells**
762 P14 and/or polyclonal WT (CD4-Cre), WT Nur77-GFP, P2RX7-KO (CD4-Cre *P2rx7*$^{fl/fl}$) or
763 Panx1-KO (CD4-Cre *Panx1*$^{fl/fl}$) $CD8^+$ T cells were isolated from naïve mice with the Mouse $CD8^+$
764 T cell isolation kit (Miltenyi Biotec). Cells were stimulated for 3h, 24h, 48h or 72h with plate-
765 bound αCD3 (10 µg/ml), plate-bound αCD28 (20 µg/ml) and soluble IL-2 (10 ng/ml). When
766 indicated, ATP (50 µM, Sigma-Aldrich), Trovafloxacin (Sigma-Aldrich, 10 µM), A-438079
767 (Tocris, 10 µM), 5-BDBD (Sigma-Aldrich, 10 µM), Sodium Lactate (1 mM, Sigma-Aldrich), VB-
768 124 (10 µM, Tocris), Oligomycin (1.39 nM, Agilent), BSA-conjugated Oleic Acid (100 µM,
769 ThermoFisher), Inostamycin (0.2 µg/ml, Cayman Chemical), Glucose (Sigma-Aldrich, 1 mM) or
770 SR13800 (10 µM, Cayman Chemical) were added to the cultures at the beginning of activation.
771 In screening experiments, multiple other compounds were added to the cultures, or in
772 alternative their respective vehicles. In some experiments, after 72h of activation, $CD8^+$ T cells
773 were incubated for an additional 72h with either recombinant IL-2 (10 ng/ml) or IL-15 (10 ng/ml).
774 In some experiments, CD4-Cre or CD4-Cre *Panx1*$^{fl/fl}$ $CD8^+$ T cells were activated *in vitro* for 3h
775 with PMA and Ionomycin (Cell Stimulation Cocktail, ThermoFisher).
776
777 **Western Blot**
778 The indicated $CD8^+$ T cells were lysed in RIPA buffer supplemented with 1 mM PMSF and
779 protease/phosphatase inhibitors. Cell lysates were then sonicated, and protein concentration
780 measured using colorimetric BCA assay. Aliquots of 25 µg of protein were run on 4-12%

781 gradient agarose gels and transferred to nitrocellulose membranes using a Trans-Blot Turbo
782 system. Membranes with transferred proteins were blocked for 30 minutes at room temperature
783 with TBS, then stained with primary rabbit anti-Pannexin-1 (Cell Signaling Technologies) at
784 1/1000 dilution or mouse anti-Tubulin (Millipore) at 1/3000 dilution, at 4$^{o}$C, overnight with
785 rotation. After washing, membranes were stained with secondary anti-rabbit or anti-mouse
786 antibodies (1/15000 dilution, 1h at room temperature). After washing, membranes were imaged
787 using a LICOR Odyseey DLx system.
788
789 **Flow cytometry**
790 Lymphocytes were isolated from tissues including thymus, spleen, inguinal lymph nodes,
791 cervical lymph nodes, blood, small intestine epithelium (SI IEL), salivary glands (SG), tumors,
792 lungs and kidneys as previously described [32,37,60]. In summary, organs were removed and cut in
793 small pieces into Erlenmeyer flasks containing 30 mL of 0.5 mg/ml Collagenase type I solution
794 (tumor, kidney, and SG), 0.5 mg/ml Collagenase type IV (lung) or 0.15 mg/ml Dithioerythritol (SI
795 IEL). Following this period, lymphocytes were isolated by 44/67% Percoll gradient isolation.
796 During isolation of lymphocytes from non-lymphoid tissues, in all experiments, 50 µg of Treg-
797 Protector (anti-ARTC2.2) nanobodies (BioLegend) were injected i.v. 30 minutes prior to mouse
798 sacrifice [35]. Direct *ex vivo* staining and intracellular staining were performed as described [32]. To
799 identify LCMV-specific or Flu-specific CD8$^{+}$ T cells, tetramers were obtained from the Yerkes
800 NIH Tetramer Core: D$^{b}$-gp33 and D$^{b}$-NP-flu tetramers conjugated with APC- or PE-Streptavidin
801 were used. For detection of vascular-associated lymphocytes in non-lymphoid organs, *in vivo*
802 i.v. injection of PerCP-Cy5.5-conjugated CD8α antibody was performed [81]. Among LCMV- or
803 Flu-specific CD8$^{+}$ T cells, the following markers were used to distinguish these respective
804 populations: naïve (CD44$^{-}$CD62L$^{+}$), Tcm (CD44$^{+}$CD62L$^{+}$), Tem (CD44$^{+}$CD62L$^{-}$CD127$^{+}$), LLEC
805 (CD44$^{+}$CD62L$^{-}$CD127$^{-}$KLRG1$^{hi}$), Trm (i.v.CD8α$^{-}$CD69$^{+/-}$CD103$^{hi/int/lo}$), MPs (CD127$^{+}$KLRG1$^{-)}$,
806 TEs (CD127$^{-}$KLRG1$^{+}$). Adoptively transferred P14 cells and LCMV-specific CD8$^{+}$ T cells in

807 mixed bone marrow chimeras were identified using a combination of CD45.1 and CD45.2
808 monoclonal antibodies. In some experiments, To-Pro 3 (Sigma-Aldrich) was added right before
809 flow cytometry [22]. From *in vitro*-activated $CD8^+$ T cells, we used antibodies for CD44, CD69,
810 CD25; in some experiments, $CD8^+$ T cells were stained with Cell Trace Violet (Life
811 Technologies) according to manufacturer's instructions, for tracking of proliferation cycles. In all
812 flow cytometry experiments, Live/Dead Near-IR was used to distinguish between live and dead
813 cells. Intracellular detection of Ki-67 and IFNγ was done as described before [32]. For
814 mitochondrial mass and membrane potential measurements, cells were incubated with Mito
815 Green (Thermo Fisher Scientific) and Mitotracker Deep Red (Thermo Fisher Scientific) or TMRE
816 (Cell Signaling Technology) simultaneously for 15 min at 37°C prior to staining. For intracellular
817 detection of phosphorylated Acetyl-CoA Carboxylase (pACC; Cell Signaling Technology) or
818 phosphorylated ERK1/2 (pERK1/2; Biolegend), cells were stained with surface markers then
819 fixed with Paraformaldehyde 1%, permeabilized with 90% Methanol and stained with pACC or
820 pERK1/2-PE for 20 min at room temperature. A secondary antibody (Alexa Fluor 647 anti-rabbit
821 IgG) was used for detection of pACC. Alexa Fluor 488-conjugated Cholera Toxin B was used for
822 detection of lipid rafts and stained as described in [49]. Nur77 was detected as GFP signal from
823 Nur77-GFP cells via flow cytometry. Apoptosis (cleaved Caspase 3/7) measurements were
824 done using the FMK-FLICA-Caspase 3/7 Kit (+ PI staining; Thermo Fisher Scientific) following
825 the manufacturer instructions. Flow cytometric analyses were performed on FACS Symphony or
826 LSR Fortessa (BD Biosciences) and data was analyzed using FlowJo software (Treestar).
827

828 **Cell sorting**

829 Cell sorting was performed on a FACS Aria III device (BD Biosciences). RNA-seq analysis
830 experiments were performed on WT (CD4-Cre) and Panx1-KO (CD4-Cre *Panx1*$^{fl/fl}$) TE
831 ($KLRG1^+CD127^-$) and MP ($KLRG1^-CD127^+$) P14 cells sorted from mice 7 days post-LCMV
832 infection. The population purity after cell sorting was > 98% in all experiments.

833

834 **Intracellular and extracellular ATP measurements**

835 Intracellular ATP concentrations were measured by using the ATP determination kit (Life
836 Technologies). To assess the levels of extracellular ATP, WT $CD8^+$ T cells were activated *in*
837 *vitro* as described above, and further incubated with IL-2 for 24h; IL-2 incubation cultures were
838 performed in Transwells (Corning). After 24 h of IL-2 incubation, the transwells were transferred
839 to new wells and the plates were centrifuged at 50 rpm for 1 min. The supernatant below the
840 transwells was quantified for ATP concentration as described above. In all transwells, a
841 combination of the plasma membrane ATPase inhibitor Ebselen (30 μM; Cayman Chemical)
842 and the ecto-ATPase inhibitor ARL 67156 trisodium salt hydrate (100 μM; Sigma-Aldrich) was
843 added 1 h before evaluation, to inhibit ATPase activity [32]. In some samples, Trovafloxacin (10
844 μM) was added 24 h before assessment.

845

846 **CRISPR-Cas9 experiments**

847 Cas9/RNP nucleofection of P14 cells was performed as previously described[53]. Briefly, WT
848 (CD4-Cre) and CD4-Cre *P2rx7*$^{fl/fl}$ P14 cells were isolated and activated as described above.
849 After 24h of activation, single guide RNAs (sgRNA) for either *Cd4* (sg*Cd4*), *Panx1* (sg*Panx1*) or
850 *P2rx4* (sg*P2rx4*) and Cas9 protein were pre-complexed at room temperature for at least 10
851 mins. Following this, 1-10 million of pre-activated P14 cells were resuspended in 20 μl of P4
852 Nucleofection Buffer (Lonza). This cell suspension was then mixed with sgRNA/Cas9 and then
853 incubated at room temperature for 2 mins. The P14 cell/Cas9/RNP mixes were transferred to
854 Nucleofection cuvette strips (4D-Nucleofector X kit S; Lonza). Cells were electroporated using a
855 4D nucleofector (4D-Nucleofector Core Unit; Lonza). After nucleofection, prewarmed complete
856 RPMI was used to transfer transfected P14 cells in 96-well plates. After 2h, P14 cells were
857 cultured in 24-well plates in complete RPMI for 48 h, before transfer into recipient mice.

858

859 **RNA-seq and bioinformatics analyses**

860 WT (CD4-Cre) or CD4-Cre *Panx1*$^{fl/fl}$ P14 cells were *in vitro* activated for 72h ("effector-like") or
861 activated and subsequently treated with recombinant IL-15 ("memory-like"). In another
862 experiment, CD4-Cre or CD4-Cre *Panx1*$^{fl/fl}$ TE or MP cells were sorted from mice infected with
863 LCMV-Arm (7 days p.i.). These cells were homogenized using QIAshredder columns (Qiagen),
864 and RNA was extracted using the RNeasy Plus Mini Kit (Qiagen) following the manufacturer's
865 instructions. Library preparation and RNA-seq (BGI-Seq platform, PE 100-bp paired-end read
866 length) was done by BGI Americas. RNA-seq reads were mapped, and raw count matrix was
867 generated. DEG analysis was done using DESeq2, and genes with greater than twofold
868 changes and false discovery rate <0.05 were considered for gene cluster analysis. BGI provided
869 customized analysis of DEGs, principal component analysis plots, and Pathway analyses
870 between groups. Some heatmaps were generated using the Morpheus software (Broad
871 Institute; https://software.broadinstitute.org/morpheus/). Some RNA-seq expression value
872 counts were collected from the public database ImmGen (immgen.org), and from previous RNA-
873 seq analysis performed by our group [32,34]. These RNA-seq analyses can be accessed at GEO
874 Omnibus with the accession numbers GSE217292 and GSE218643. Analysis of single-cell
875 RNA-seq from spleen P14 cells from days 3 or 7 after LCMV-Arm infection[82] (GSE131847) was
876 done using R Studio.

877

878 **Extracellular flux analyses**

879 In the indicated naïve, *in vitro*-activated or *ex vivo*-sorted CD8$^{+}$ T cell populations, OCR and
880 ECAR values were measured using a 96-well XF Extracellular flux analyzer, following
881 manufacturer instructions (Agilent). Spare respiratory capacity (SRC) was defined as the
882 subtraction between the maximum OCR values and the baseline OCR values [32,37].

883

884 **Metabolomics analyses**

885 For untargeted metabolomics, the indicated *in vitro*-activated $CD8^+$ T cell populations were
886 isolated. We separated cell pellets and supernatants and sent them to the Mayo Clinic
887 Metabolomics Core Laboratory for Liquid Chromatography-Mass Spectrometry (LC-MS)
888 metabolome assessments. Primary analyses and comparisons of differentially expressed
889 metabolites (DEMs) were done by the Metabolomics Core. Pathway enrichment analyses of
890 DEMs were done using the MetaboAnalyst tool. Heatmaps of the top-100 DEMs for each
891 comparison were generated using the Morpheus software. For targeted metabolomics analyses,
892 *in vitro*-activated $CD8^+$ T cells will be cultured for the final 12h of activation with $^{13}C$-Glucose
893 (Cambridge Isotopes) or $^{13}C$-Sodium Lactate (Cambridge Isotopes). We separated cell pellets
894 and sent them to the Mayo Clinic Metabolomics Core Laboratory for metabolome assessments
895 of the TCA cycle.
896
897 **L-lactate detection assays**
898 When indicated, the supernatants from *in vitro*-activated $CD8^+$ T cell populations or serum from
899 LCMV-infected mice were collected, and the concentrations of extracellular L-lactate were
900 measured using the L-Lactate Assay Kit (Sigma-Aldrich), following the manufacturer's
901 instructions.
902
903 **Quantification and statistical analyses**
904 Details on statistics used can be found in figure legends. Data were subjected to the
905 Kolmogorov-Smirnov test to assess normality of samples. Statistical differences were calculated
906 by using unpaired two-tailed Student's t-test, one-way ANOVA with Tukey post-test, two-way
907 ANOVA with Bonferroni's post-test, or Kaplan-Meier survival curve analysis. All experiments
908 were analyzed using Prism 10 (GraphPad Software). Graphical data was shown as mean
909 values with error bars indicating the SD. P values of $< 0.05$ (*), $< 0.01$ (*), $< 0.001$ (***) or $<$
910 $0.0001$ (****) indicated significant differences between groups.

**Supplementary Materials:** This article includes Figs.S1 to S7.

937 **References**
938

939 1. Harty, J.T., Tvinnereim, A.R., and White, D.W. (2000). CD8+ T cell effector mechanisms
940 in resistance to infection. Annu Rev Immunol *18*, 275-308.
941 10.1146/annurev.immunol.18.1.275.
942 2. Williams, M.A., and Bevan, M.J. (2007). Effector and memory CTL differentiation. Annu
943 Rev Immunol *25*, 171-192. 10.1146/annurev.immunol.25.022106.141548.
944 3. Renkema, K.R., Huggins, M.A., Borges da Silva, H., Knutson, T.P., Henzler, C.M., and
945 Hamilton, S.E. (2020). KLRG1(+) Memory CD8 T Cells Combine Properties of Short-
946 Lived Effectors and Long-Lived Memory. J Immunol *205*, 1059-1069.
947 10.4049/jimmunol.1901512.
948 4. Milner, J.J., Nguyen, H., Omilusik, K., Reina-Campos, M., Tsai, M., Toma, C., Delpoux,
949 A., Boland, B.S., Hedrick, S.M., Chang, J.T., and Goldrath, A.W. (2020). Delineation of a
950 molecularly distinct terminally differentiated memory CD8 T cell population. Proc Natl
951 Acad Sci U S A *117*, 25667-25678. 10.1073/pnas.2008571117.
952 5. Jameson, S.C., and Masopust, D. (2018). Understanding Subset Diversity in T Cell
953 Memory. Immunity *48*, 214-226. 10.1016/j.immuni.2018.02.010.
954 6. Masopust, D., and Soerens, A.G. (2019). Tissue-Resident T Cells and Other Resident
955 Leukocytes. Annu Rev Immunol *37*, 521-546. 10.1146/annurev-immunol-042617-
956 053214.
957 7. Chen, L., and Flies, D.B. (2013). Molecular mechanisms of T cell co-stimulation and co-
958 inhibition. Nat Rev Immunol *13*, 227-242. 10.1038/nri3405.
959 8. Leal, J.M., Huang, J.Y., Kohli, K., Stoltzfus, C., Lyons-Cohen, M.R., Olin, B.E., Gale, M.,
960 Jr., and Gerner, M.Y. (2021). Innate cell microenvironments in lymph nodes shape the
961 generation of T cell responses during type I inflammation. Sci Immunol *6*.
962 10.1126/sciimmunol.abb9435.
963 9. Kapsenberg, M.L. (2003). Dendritic-cell control of pathogen-driven T-cell polarization.
964 Nat Rev Immunol *3*, 984-993. 10.1038/nri1246.
965 10. Williams, M.A., Tyznik, A.J., and Bevan, M.J. (2006). Interleukin-2 signals during priming
966 are required for secondary expansion of CD8+ memory T cells. Nature *441*, 890-893.
967 10.1038/nature04790.
968 11. Kaech, S.M., Tan, J.T., Wherry, E.J., Konieczny, B.T., Surh, C.D., and Ahmed, R.
969 (2003). Selective expression of the interleukin 7 receptor identifies effector CD8 T cells
970 that give rise to long-lived memory cells. Nat Immunol *4*, 1191-1198. 10.1038/ni1009.
971 12. Ku, C.C., Murakami, M., Sakamoto, A., Kappler, J., and Marrack, P. (2000). Control of
972 homeostasis of CD8+ memory T cells by opposing cytokines. Science *288*, 675-678.
973 10.1126/science.288.5466.675.
974 13. Zhang, N., and Bevan, M.J. (2013). Transforming growth factor-beta signaling controls
975 the formation and maintenance of gut-resident memory T cells by regulating migration
976 and retention. Immunity *39*, 687-696. 10.1016/j.immuni.2013.08.019.
977 14. Chan, F.K., Luz, N.F., and Moriwaki, K. (2015). Programmed necrosis in the cross talk of
978 cell death and inflammation. Annu Rev Immunol *33*, 79-106. 10.1146/annurev-immunol-
979 032414-112248.
980 15. Syrjanen, J., Michalski, K., Kawate, T., and Furukawa, H. (2021). On the molecular
981 nature of large-pore channels. J Mol Biol *433*, 166994. 10.1016/j.jmb.2021.166994.
982 16. Molica, F., Figueroa, X.F., Kwak, B.R., Isakson, B.E., and Gibbins, J.M. (2018).
983 Connexins and Pannexins in Vascular Function and Disease. Int J Mol Sci *19*.
984 10.3390/ijms19061663.
985 17. Mese, G., Richard, G., and White, T.W. (2007). Gap junctions: basic structure and
986 function. J Invest Dermatol *127*, 2516-2524. 10.1038/sj.jid.5700770.

18. Bhat, E.A., and Sajjad, N. (2021). Human Pannexin 1 channel: Insight in structure-function mechanism and its potential physiological roles. Mol Cell Biochem *476*, 1529-1540. 10.1007/s11010-020-04002-3.
19. Narahari, A.K., Kreutzberger, A.J., Gaete, P.S., Chiu, Y.H., Leonhardt, S.A., Medina, C.B., Jin, X., Oleniacz, P.W., Kiessling, V., Barrett, P.Q., et al. (2021). ATP and large signaling metabolites flux through caspase-activated Pannexin 1 channels. Elife *10*. 10.7554/eLife.64787.
20. Chekeni, F.B., Elliott, M.R., Sandilos, J.K., Walk, S.F., Kinchen, J.M., Lazarowski, E.R., Armstrong, A.J., Penuela, S., Laird, D.W., Salvesen, G.S., et al. (2010). Pannexin 1 channels mediate 'find-me' signal release and membrane permeability during apoptosis. Nature *467*, 863-867. 10.1038/nature09413.
21. Medina, C.B., Mehrotra, P., Arandjelovic, S., Perry, J.S.A., Guo, Y., Morioka, S., Barron, B., Walk, S.F., Ghesquiere, B., Krupnick, A.S., et al. (2020). Metabolites released from apoptotic cells act as tissue messengers. Nature *580*, 130-135. 10.1038/s41586-020-2121-3.
22. Poon, I.K., Chiu, Y.H., Armstrong, A.J., Kinchen, J.M., Juncadella, I.J., Bayliss, D.A., and Ravichandran, K.S. (2014). Unexpected link between an antibiotic, pannexin channels and apoptosis. Nature *507*, 329-334. 10.1038/nature13147.
23. Beckel, J.M., Daugherty, S.L., Tyagi, P., Wolf-Johnston, A.S., Birder, L.A., Mitchell, C.H., and de Groat, W.C. (2015). Pannexin 1 channels mediate the release of ATP into the lumen of the rat urinary bladder. J Physiol *593*, 1857-1871. 10.1113/jphysiol.2014.283119.
24. Chiu, Y.H., Jin, X., Medina, C.B., Leonhardt, S.A., Kiessling, V., Bennett, B.C., Shu, S., Tamm, L.K., Yeager, M., Ravichandran, K.S., and Bayliss, D.A. (2017). A quantized mechanism for activation of pannexin channels. Nat Commun *8*, 14324. 10.1038/ncomms14324.
25. Iglesias, R., Locovei, S., Roque, A., Alberto, A.P., Dahl, G., Spray, D.C., and Scemes, E. (2008). P2X7 receptor-Pannexin1 complex: pharmacology and signaling. Am J Physiol Cell Physiol *295*, C752-760. 10.1152/ajpcell.00228.2008.
26. Silverman, W.R., de Rivero Vaccari, J.P., Locovei, S., Qiu, F., Carlsson, S.K., Scemes, E., Keane, R.W., and Dahl, G. (2009). The pannexin 1 channel activates the inflammasome in neurons and astrocytes. J Biol Chem *284*, 18143-18151. 10.1074/jbc.M109.004804.
27. Weilinger, N.L., Lohman, A.W., Rakai, B.D., Ma, E.M., Bialecki, J., Maslieieva, V., Rilea, T., Bandet, M.V., Ikuta, N.T., Scott, L., et al. (2016). Metabotropic NMDA receptor signaling couples Src family kinases to pannexin-1 during excitotoxicity. Nat Neurosci *19*, 432-442. 10.1038/nn.4236.
28. Woehrle, T., Yip, L., Elkhal, A., Sumi, Y., Chen, Y., Yao, Y., Insel, P.A., and Junger, W.G. (2010). Pannexin-1 hemichannel-mediated ATP release together with P2X1 and P2X4 receptors regulate T-cell activation at the immune synapse. Blood *116*, 3475-3484. 10.1182/blood-2010-04-277707.
29. Woehrle, T., Yip, L., Manohar, M., Sumi, Y., Yao, Y., Chen, Y., and Junger, W.G. (2010). Hypertonic stress regulates T cell function via pannexin-1 hemichannels and P2X receptors. J Leukoc Biol *88*, 1181-1189. 10.1189/jlb.0410211.
30. Medina, C.B., Chiu, Y.H., Stremska, M.E., Lucas, C.D., Poon, I., Tung, K.S., Elliott, M.R., Desai, B., Lorenz, U.M., Bayliss, D.A., and Ravichandran, K.S. (2021). Pannexin 1 channels facilitate communication between T cells to restrict the severity of airway inflammation. Immunity *54*, 1715-1727 e1717. 10.1016/j.immuni.2021.06.014.
31. Schenk, U., Westendorf, A.M., Radaelli, E., Casati, A., Ferro, M., Fumagalli, M., Verderio, C., Buer, J., Scanziani, E., and Grassi, F. (2008). Purinergic control of T cell

1037 activation by ATP released through pannexin-1 hemichannels. Sci Signal *1*, ra6.
1038 10.1126/scisignal.1160583.
1039 32. Borges da Silva, H., Beura, L.K., Wang, H., Hanse, E.A., Gore, R., Scott, M.C., Walsh,
1040 D.A., Block, K.E., Fonseca, R., Yan, Y., et al. (2018). The purinergic receptor P2RX7
1041 directs metabolic fitness of long-lived memory CD8(+) T cells. Nature *559*, 264-268.
1042 10.1038/s41586-018-0282-0.
1043 33. Di Virgilio, F., Dal Ben, D., Sarti, A.C., Giuliani, A.L., and Falzoni, S. (2017). The P2X7
1044 Receptor in Infection and Inflammation. Immunity *47*, 15-31.
1045 10.1016/j.immuni.2017.06.020.
1046 34. Vardam-Kaur, T., van Dijk, S., Peng, C., Wanhainen, K.M., Jameson, S.C., and Borges
1047 da Silva, H. (2022). The Extracellular ATP Receptor P2RX7 Imprints a Promemory
1048 Transcriptional Signature in Effector CD8(+) T Cells. J Immunol *208*, 1686-1699.
1049 10.4049/jimmunol.2100555.
1050 35. Borges da Silva, H., Wang, H., Qian, L.J., Hogquist, K.A., and Jameson, S.C. (2019).
1051 ARTC2.2/P2RX7 Signaling during Cell Isolation Distorts Function and Quantification of
1052 Tissue-Resident CD8(+) T Cell and Invariant NKT Subsets. J Immunol *202*, 2153-2163.
1053 10.4049/jimmunol.1801613.
1054 36. Stark, R., Wesselink, T.H., Behr, F.M., Kragten, N.A.M., Arens, R., Koch-Nolte, F., van
1055 Gisbergen, K., and van Lier, R.A.W. (2018). T RM maintenance is regulated by tissue
1056 damage via P2RX7. Sci Immunol *3*. 10.1126/sciimmunol.aau1022.
1057 37. Borges da Silva, H., Peng, C., Wang, H., Wanhainen, K.M., Ma, C., Lopez, S., Khoruts,
1058 A., Zhang, N., and Jameson, S.C. (2020). Sensing of ATP via the Purinergic Receptor
1059 P2RX7 Promotes CD8(+) Trm Cell Generation by Enhancing Their Sensitivity to the
1060 Cytokine TGF-beta. Immunity *53*, 158-171 e156. 10.1016/j.immuni.2020.06.010.
1061 38. Taruno, A. (2018). ATP Release Channels. Int J Mol Sci *19*. 10.3390/ijms19030808.
1062 39. Chang, C.H., Curtis, J.D., Maggi, L.B., Jr., Faubert, B., Villarino, A.V., O'Sullivan, D.,
1063 Huang, S.C., van der Windt, G.J., Blagih, J., Qiu, J., et al. (2013). Posttranscriptional
1064 control of T cell effector function by aerobic glycolysis. Cell *153*, 1239-1251.
1065 10.1016/j.cell.2013.05.016.
1066 40. Reina-Campos, M., Scharping, N.E., and Goldrath, A.W. (2021). CD8(+) T cell
1067 metabolism in infection and cancer. Nat Rev Immunol *21*, 718-738. 10.1038/s41577-
1068 021-00537-8.
1069 41. Carrio, R., Bathe, O.F., and Malek, T.R. (2004). Initial antigen encounter programs CD8+
1070 T cells competent to develop into memory cells that are activated in an antigen-free, IL-
1071 7- and IL-15-rich environment. J Immunol *172*, 7315-7323.
1072 10.4049/jimmunol.172.12.7315.
1073 42. Brock, V.J., Wolf, I.M.A., Er-Lukowiak, M., Lory, N., Stahler, T., Woelk, L.M., Mittrucker,
1074 H.W., Muller, C.E., Koch-Nolte, F., Rissiek, B., et al. (2022). P2X4 and P2X7 are
1075 essential players in basal T cell activity and Ca(2+) signaling milliseconds after T cell
1076 activation. Sci Adv *8*, eabl9770. 10.1126/sciadv.abl9770.
1077 43. Kaymak, I., Luda, K.M., Duimstra, L.R., Ma, E.H., Longo, J., Dahabieh, M.S., Faubert,
1078 B., Oswald, B.M., Watson, M.J., Kitchen-Goosen, S.M., et al. (2022). Carbon source
1079 availability drives nutrient utilization in CD8(+) T cells. Cell Metab *34*, 1298-1311 e1296.
1080 10.1016/j.cmet.2022.07.012.
1081 44. Barbieri, L., Velica, P., Gameiro, P.A., Cunha, P.P., Foskolou, I.P., Rullman, E.,
1082 Bargiela, D., Johnson, R.S., and Rundqvist, H. (2023). Lactate exposure shapes the
1083 metabolic and transcriptomic profile of CD8+ T cells. Front Immunol *14*, 1101433.
1084 10.3389/fimmu.2023.1101433.
1085 45. Macchi, C., Moregola, A., Greco, M.F., Svecla, M., Bonacina, F., Dhup, S., Dadhich,
1086 R.K., Audano, M., Sonveaux, P., Mauro, C., et al. (2022). Monocarboxylate transporter 1

1087 deficiency impacts CD8(+) T lymphocytes proliferation and recruitment to adipose tissue
1088 during obesity. iScience *25*, 104435. 10.1016/j.isci.2022.104435.
1089 46. Brand, A., Singer, K., Koehl, G.E., Kolitzus, M., Schoenhammer, G., Thiel, A., Matos, C.,
1090 Bruss, C., Klobuch, S., Peter, K., et al. (2016). LDHA-Associated Lactic Acid Production
1091 Blunts Tumor Immunosurveillance by T and NK Cells. Cell Metab *24*, 657-671.
1092 10.1016/j.cmet.2016.08.011.
1093 47. Wu, N., Yang, M., Gaur, U., Xu, H., Yao, Y., and Li, D. (2016). Alpha-Ketoglutarate:
1094 Physiological Functions and Applications. Biomol Ther (Seoul) *24*, 1-8.
1095 10.4062/biomolther.2015.078.
1096 48. Williams, N.C., and O'Neill, L.A.J. (2018). A Role for the Krebs Cycle Intermediate
1097 Citrate in Metabolic Reprogramming in Innate Immunity and Inflammation. Front
1098 Immunol *9*, 141. 10.3389/fimmu.2018.00141.
1099 49. Edwards-Hicks, J., Apostolova, P., Buescher, J.M., Maib, H., Stanczak, M.A., Corrado,
1100 M., Klein Geltink, R.I., Maccari, M.E., Villa, M., Carrizo, G.E., et al. (2023).
1101 Phosphoinositide acyl chain saturation drives CD8(+) effector T cell signaling and
1102 function. Nat Immunol *24*, 516-530. 10.1038/s41590-023-01419-y.
1103 50. Rowlatt, B., Yorke, J.A., Strong, A.J., Whitehouse, C.J., Bell, S.G., and Wong, L.L.
1104 (2011). Chain length-dependent cooperativity in fatty acid binding and oxidation by
1105 cytochrome P450BM3 (CYP102A1). Protein Cell *2*, 656-671. 10.1007/s13238-011-1082-
1106 6.
1107 51. Huang, Y.H., and Sauer, K. (2010). Lipid signaling in T-cell development and function.
1108 Cold Spring Harb Perspect Biol *2*, a002428. 10.1101/cshperspect.a002428.
1109 52. Yip, L., Woehrle, T., Corriden, R., Hirsh, M., Chen, Y., Inoue, Y., Ferrari, V., Insel, P.A.,
1110 and Junger, W.G. (2009). Autocrine regulation of T-cell activation by ATP release and
1111 P2X7 receptors. FASEB J *23*, 1685-1693. 10.1096/fj.08-126458.
1112 53. Seki, A., and Rutz, S. (2018). Optimized RNP transfection for highly efficient
1113 CRISPR/Cas9-mediated gene knockout in primary T cells. J Exp Med *215*, 985-997.
1114 10.1084/jem.20171626.
1115 54. Blagih, J., Coulombe, F., Vincent, E.E., Dupuy, F., Galicia-Vazquez, G., Yurchenko, E.,
1116 Raissi, T.C., van der Windt, G.J., Viollet, B., Pearce, E.L., et al. (2015). The energy
1117 sensor AMPK regulates T cell metabolic adaptation and effector responses in vivo.
1118 Immunity *42*, 41-54. 10.1016/j.immuni.2014.12.030.
1119 55. Pearce, E.L., Poffenberger, M.C., Chang, C.H., and Jones, R.G. (2013). Fueling
1120 immunity: insights into metabolism and lymphocyte function. Science *342*, 1242454.
1121 10.1126/science.1242454.
1122 56. Huang, A.C., Postow, M.A., Orlowski, R.J., Mick, R., Bengsch, B., Manne, S., Xu, W.,
1123 Harmon, S., Giles, J.R., Wenz, B., et al. (2017). T-cell invigoration to tumour burden ratio
1124 associated with anti-PD-1 response. Nature *545*, 60-65. 10.1038/nature22079.
1125 57. Pentcheva-Hoang, T., Simpson, T.R., Montalvo-Ortiz, W., and Allison, J.P. (2014).
1126 Cytotoxic T lymphocyte antigen-4 blockade enhances antitumor immunity by stimulating
1127 melanoma-specific T-cell motility. Cancer Immunol Res *2*, 970-980. 10.1158/2326-
1128 6066.CIR-14-0104.
1129 58. Yuan, J., Adamow, M., Ginsberg, B.A., Rasalan, T.S., Ritter, E., Gallardo, H.F., Xu, Y.,
1130 Pogoriler, E., Terzulli, S.L., Kuk, D., et al. (2011). Integrated NY-ESO-1 antibody and
1131 CD8+ T-cell responses correlate with clinical benefit in advanced melanoma patients
1132 treated with ipilimumab. Proc Natl Acad Sci U S A *108*, 16723-16728.
1133 10.1073/pnas.1110814108.
1134 59. Curtsinger, J.M., Gerner, M.Y., Lins, D.C., and Mescher, M.F. (2007). Signal 3
1135 availability limits the CD8 T cell response to a solid tumor. J Immunol *178*, 6752-6760.
1136 10.4049/jimmunol.178.11.6752.

1137 60. Wanhainen, K.M., Peng, C., Zhou, M.H., Macedo, B.G., O'Flanagan, S., Yang, T.,
1138 Kelekar, A., Burbach, B.J., Borges da Silva, H., and Jameson, S.C. (2022). P2RX7
1139 Enhances Tumor Control by CD8+ T Cells in Adoptive Cell Therapy. Cancer Immunol
1140 Res *10*, 871-884. 10.1158/2326-6066.CIR-21-0691.
1141 61. van Leeuwen, L., Guiffre, A., Atkinson, K., Rainer, S.P., and Sewell, W.A. (2002). A two-
1142 phase pathogenesis of graft-versus-host disease in mice. Bone Marrow Transplant *29*,
1143 151-158. 10.1038/sj.bmt.1703328.
1144 62. Carr, E.L., Kelman, A., Wu, G.S., Gopaul, R., Senkevitch, E., Aghvanyan, A., Turay,
1145 A.M., and Frauwirth, K.A. (2010). Glutamine uptake and metabolism are coordinately
1146 regulated by ERK/MAPK during T lymphocyte activation. J Immunol *185*, 1037-1044.
1147 10.4049/jimmunol.0903586.
1148 63. Hayashi, K., Jutabha, P., Endou, H., Sagara, H., and Anzai, N. (2013). LAT1 is a critical
1149 transporter of essential amino acids for immune reactions in activated human T cells. J
1150 Immunol *191*, 4080-4085. 10.4049/jimmunol.1300923.
1151 64. Ma, E.H., Verway, M.J., Johnson, R.M., Roy, D.G., Steadman, M., Hayes, S., Williams,
1152 K.S., Sheldon, R.D., Samborska, B., Kosinski, P.A., et al. (2019). Metabolic Profiling
1153 Using Stable Isotope Tracing Reveals Distinct Patterns of Glucose Utilization by
1154 Physiologically Activated CD8(+) T Cells. Immunity *51*, 856-870 e855.
1155 10.1016/j.immuni.2019.09.003.
1156 65. Ledderose, C., Bromberger, S., Slubowski, C.J., Sueyoshi, K., and Junger, W.G. (2021).
1157 Frontline Science: P2Y11 receptors support T cell activation by directing mitochondrial
1158 trafficking to the immune synapse. J Leukoc Biol *109*, 497-508. 10.1002/JLB.2HI0520-
1159 191R.
1160 66. Menk, A.V., Scharping, N.E., Moreci, R.S., Zeng, X., Guy, C., Salvatore, S., Bae, H., Xie,
1161 J., Young, H.A., Wendell, S.G., and Delgoffe, G.M. (2018). Early TCR Signaling Induces
1162 Rapid Aerobic Glycolysis Enabling Distinct Acute T Cell Effector Functions. Cell Rep *22*,
1163 1509-1521. 10.1016/j.celrep.2018.01.040.
1164 67. Grist, J.T., Jarvis, L.B., Georgieva, Z., Thompson, S., Kaur Sandhu, H., Burling, K.,
1165 Clarke, A., Jackson, S., Wills, M., Gallagher, F.A., and Jones, J.L. (2018). Extracellular
1166 Lactate: A Novel Measure of T Cell Proliferation. J Immunol *200*, 1220-1226.
1167 10.4049/jimmunol.1700886.
1168 68. Haas, R., Smith, J., Rocher-Ros, V., Nadkarni, S., Montero-Melendez, T., D'Acquisto, F.,
1169 Bland, E.J., Bombardieri, M., Pitzalis, C., Perretti, M., et al. (2015). Lactate Regulates
1170 Metabolic and Pro-inflammatory Circuits in Control of T Cell Migration and Effector
1171 Functions. PLoS Biol *13*, e1002202. 10.1371/journal.pbio.1002202.
1172 69. Feng, Q., Liu, Z., Yu, X., Huang, T., Chen, J., Wang, J., Wilhelm, J., Li, S., Song, J., Li,
1173 W., et al. (2022). Lactate increases stemness of CD8 + T cells to augment anti-tumor
1174 immunity. Nat Commun *13*, 4981. 10.1038/s41467-022-32521-8.
1175 70. Robergs, R.A., Ghiasvand, F., and Parker, D. (2004). Biochemistry of exercise-induced
1176 metabolic acidosis. Am J Physiol Regul Integr Comp Physiol *287*, R502-516.
1177 10.1152/ajpregu.00114.2004.
1178 71. Wanhainen, K.M., Jameson, S.C., and da Silva, H.B. (2019). Self-Regulation of Memory
1179 CD8 T Cell Metabolism through Extracellular ATP Signaling. Immunometabolism *1*.
1180 10.20900/immunometab20190009.
1181 72. Denton, R.M. (2009). Regulation of mitochondrial dehydrogenases by calcium ions.
1182 Biochim Biophys Acta *1787*, 1309-1316. 10.1016/j.bbabio.2009.01.005.
1183 73. Proietti, M., Perruzza, L., Scribano, D., Pellegrini, G., D'Antuono, R., Strati, F., Raffaelli,
1184 M., Gonzalez, S.F., Thelen, M., Hardt, W.D., et al. (2019). ATP released by intestinal
1185 bacteria limits the generation of protective IgA against enteropathogens. Nat Commun
1186 *10*, 250. 10.1038/s41467-018-08156-z.

1187 74. Rolf, J., Zarrouk, M., Finlay, D.K., Foretz, M., Viollet, B., and Cantrell, D.A. (2013).
1188 AMPKalpha1: a glucose sensor that controls CD8 T-cell memory. Eur J Immunol *43*,
1189 889-896. 10.1002/eji.201243008.
1190 75. Quinn, W.J., 3rd, Jiao, J., TeSlaa, T., Stadanlick, J., Wang, Z., Wang, L., Akimova, T.,
1191 Angelin, A., Schafer, P.M., Cully, M.D., et al. (2020). Lactate Limits T Cell Proliferation
1192 via the NAD(H) Redox State. Cell Rep *33*, 108500. 10.1016/j.celrep.2020.108500.
1193 76. Bao, L., Sun, K., and Zhang, X. (2021). PANX1 is a potential prognostic biomarker
1194 associated with immune infiltration in pancreatic adenocarcinoma: A pan-cancer
1195 analysis. Channels (Austin) *15*, 680-696. 10.1080/19336950.2021.2004758.
1196 77. Penuela, S., Gyenis, L., Ablack, A., Churko, J.M., Berger, A.C., Litchfield, D.W., Lewis,
1197 J.D., and Laird, D.W. (2012). Loss of pannexin 1 attenuates melanoma progression by
1198 reversion to a melanocytic phenotype. J Biol Chem *287*, 29184-29193.
1199 10.1074/jbc.M112.377176.
1200 78. Huang, K.C., Chiang, S.F., Lin, P.C., Hong, W.Z., Yang, P.C., Chang, H.P., Peng, S.L.,
1201 Chen, T.W., Ke, T.W., Liang, J.A., et al. (2024). TNFalpha modulates PANX1 activation
1202 to promote ATP release and enhance P2RX7-mediated antitumor immune responses
1203 after chemotherapy in colorectal cancer. Cell Death Dis *15*, 24. 10.1038/s41419-023-
1204 06408-5.
1205 79. Vultaggio-Poma, V., Falzoni, S., Chiozzi, P., Sarti, A.C., Adinolfi, E., Giuliani, A.L.,
1206 Sanchez-Melgar, A., Boldrini, P., Zanoni, M., Tesei, A., et al. (2022). Extracellular ATP is
1207 increased by release of ATP-loaded microparticles triggered by nutrient deprivation.
1208 Theranostics *12*, 859-874. 10.7150/thno.66274.
1209 80. Elia, I., Rowe, J.H., Johnson, S., Joshi, S., Notarangelo, G., Kurmi, K., Weiss, S.,
1210 Freeman, G.J., Sharpe, A.H., and Haigis, M.C. (2022). Tumor cells dictate anti-tumor
1211 immune responses by altering pyruvate utilization and succinate signaling in CD8(+) T
1212 cells. Cell Metab *34*, 1137-1150 e1136. 10.1016/j.cmet.2022.06.008.
1213 81. Anderson, K.G., Mayer-Barber, K., Sung, H., Beura, L., James, B.R., Taylor, J.J., Qunaj,
1214 L., Griffith, T.S., Vezys, V., Barber, D.L., and Masopust, D. (2014). Intravascular staining
1215 for discrimination of vascular and tissue leukocytes. Nat Protoc *9*, 209-222.
1216 10.1038/nprot.2014.005.
1217 82. Kurd, N.S., He, Z., Louis, T.L., Milner, J.J., Omilusik, K.D., Jin, W., Tsai, M.S., Widjaja,
1218 C.E., Kanbar, J.N., Olvera, J.G., et al. (2020). Early precursors and molecular
1219 determinants of tissue-resident memory CD8(+) T lymphocytes revealed by single-cell
1220 RNA sequencing. Sci Immunol *5*. 10.1126/sciimmunol.aaz6894.
1221
1222

Figure 1

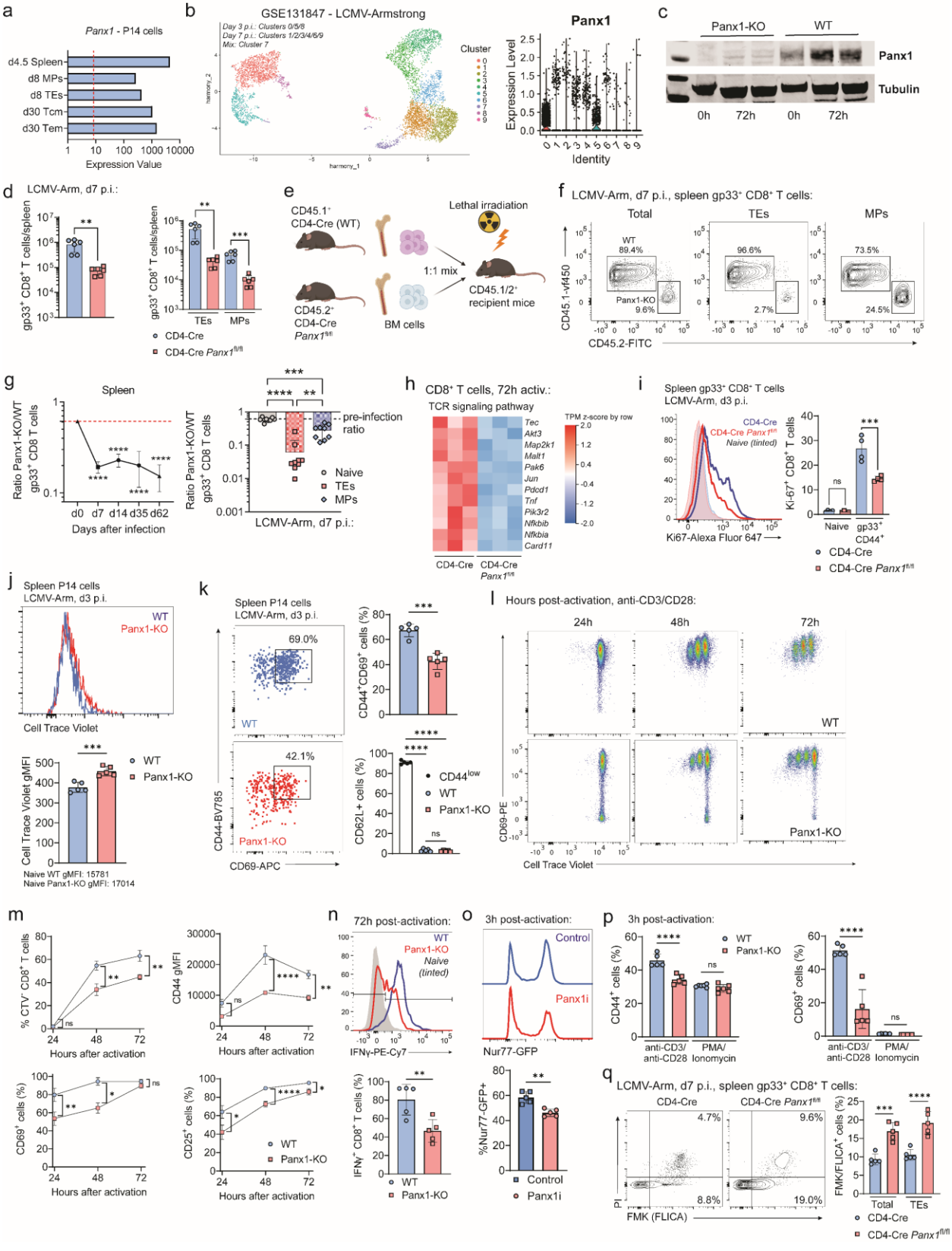
a
Panx1 - P14 cells
d4.5 Spleen
d8 MPs
d8 TEs
d30 Tcm
d30 Tem
Expression Value
b
GSE131847 - LCMV-Armstrong
Day 3 p.i.: Clusters 0/5/8
Day 7 p.i.: Clusters 1/2/3/4/6/9
Mix: Cluster 7
Cluster
Panx1
Expression Level
Identity
c
Panx1-KO
WT
Panx1
Tubulin
0h
72h
0h
72h
d
LCMV-Arm, d7 p.i.:
gp33+ CD8+ T cells/spleen
TEs
MPs
CD4-Cre
CD4-Cre Panx1fl/fl
e
CD45.1+ CD4-Cre (WT)
Lethal irradiation
1:1 mix
CD45.2+ CD4-Cre Panx1fl/fl
BM cells
CD45.1/2+ recipient mice
f
LCMV-Arm, d7 p.i., spleen gp33+ CD8+ T cells:
Total
TEs
MPs
WT 89.4%
Panx1-KO 9.6%
96.6%
2.7%
73.5%
24.5%
CD45.1-vf450
CD45.2-FITC
g
Spleen
Ratio Panx1-KO/WT gp33+ CD8 T cells
Days after infection
d0 d7 d14 d35 d62
pre-infection ratio
Naive
TEs
MPs
LCMV-Arm, d7 p.i.:
h
CD8+ T cells, 72h activ.:
TCR signaling pathway
TPM z-score by row
Tec
Akt3
Map2k1
Malt1
Pak6
Jun
Pdcd1
Tnf
Pik3r2
Nfkbib
Nfkbia
Card11
CD4-Cre
CD4-Cre Panx1fl/fl
i
Spleen gp33+ CD8+ T cells
LCMV-Arm, d3 p.i.
CD4-Cre
CD4-Cre Panx1fl/fl
Naive (tinted)
Ki67-Alexa Fluor 647
Ki-67+ CD8+ T cells
Naive
gp33+ CD44+
CD4-Cre
CD4-Cre Panx1fl/fl
j
Spleen P14 cells
LCMV-Arm, d3 p.i.
WT
Panx1-KO
Cell Trace Violet
Cell Trace Violet gMFI
Naive WT gMFI: 15781
Naive Panx1-KO gMFI: 17014
k
Spleen P14 cells
LCMV-Arm, d3 p.i.
69.0%
42.1%
WT
Panx1-KO
CD44-BV785
CD69-APC
CD44+CD69+ cells (%)
CD62L+ cells (%)
CD44low
WT
Panx1-KO
l
Hours post-activation, anti-CD3/CD28:
24h
48h
72h
WT
Panx1-KO
CD69-PE
Cell Trace Violet
m
% CTV- CD8+ T cells
Hours after activation
CD44 gMFI
CD69+ cells (%)
CD25+ cells (%)
WT
Panx1-KO
n
72h post-activation:
WT
Panx1-KO
Naive (tinted)
IFNγ-PE-Cy7
IFNγ+ CD8+ T cells (%)
WT
Panx1-KO
o
3h post-activation:
Control
Panx1i
Nur77-GFP
%Nur77-GFP+
Control
Panx1i
p
3h post-activation:
WT
Panx1-KO
CD44+ cells (%)
CD69+ cells (%)
anti-CD3/ anti-CD28
PMA/ Ionomycin
q
LCMV-Arm, d7 p.i., spleen gp33+ CD8+ T cells:
CD4-Cre
CD4-Cre Panx1fl/fl
4.7%
9.6%
8.8%
19.0%
PI
FMK (FLICA)
FMK/FLICA+ cells (%)
Total
TEs
CD4-Cre
CD4-Cre Panx1fl/fl

1226 Figure 2

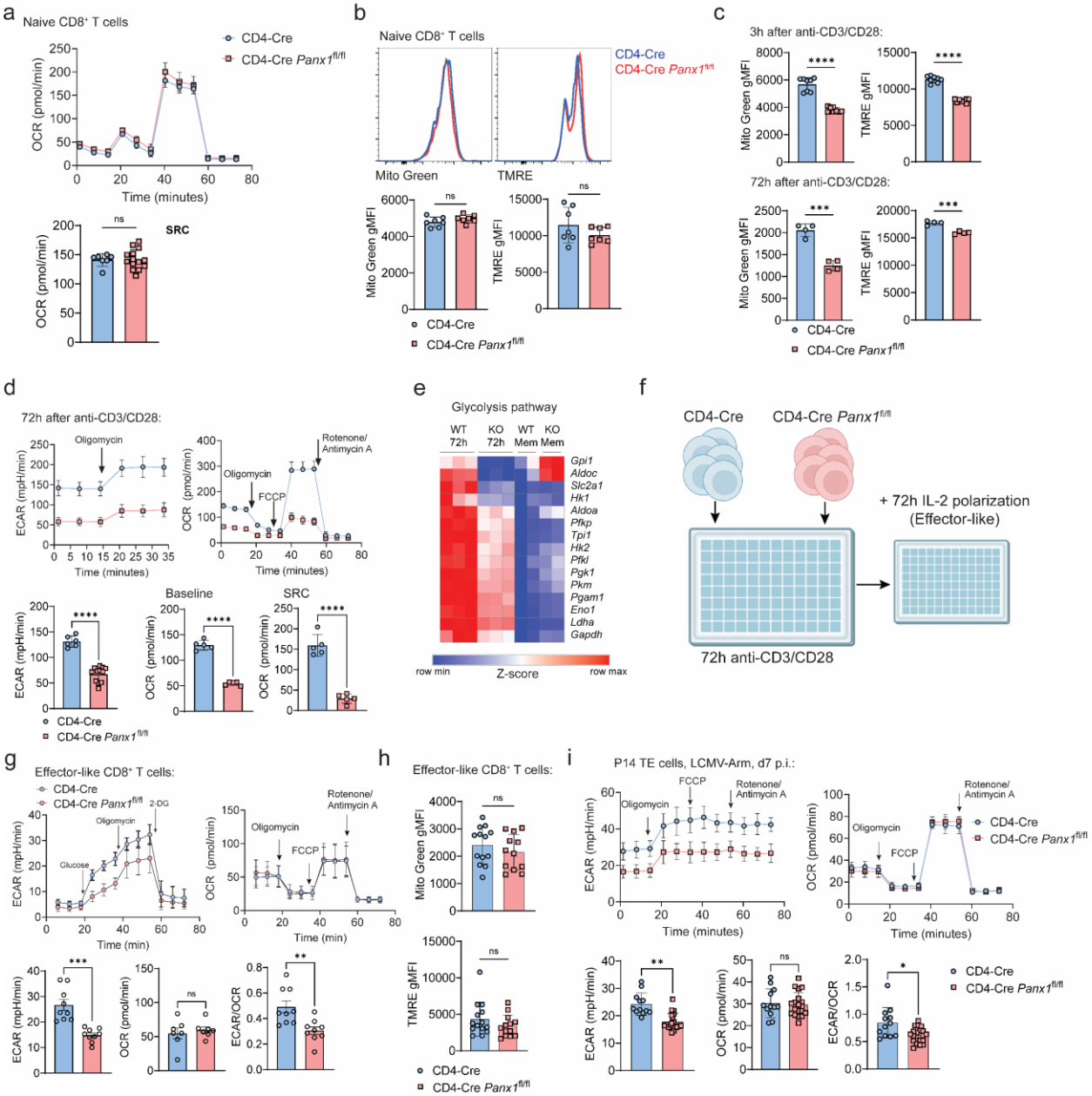


1227
1228

1229 Figure 3

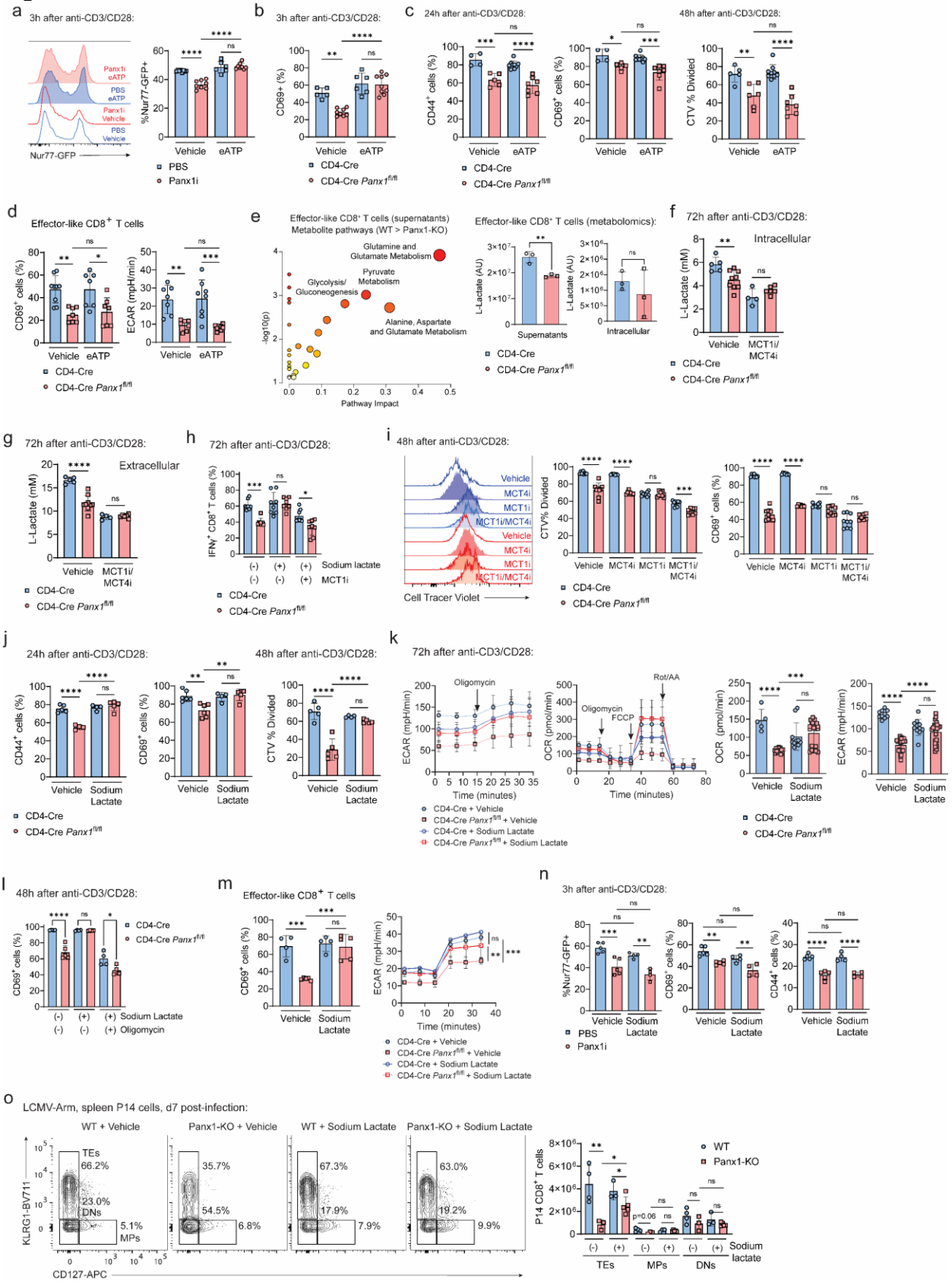


1230

1231 Figure 4

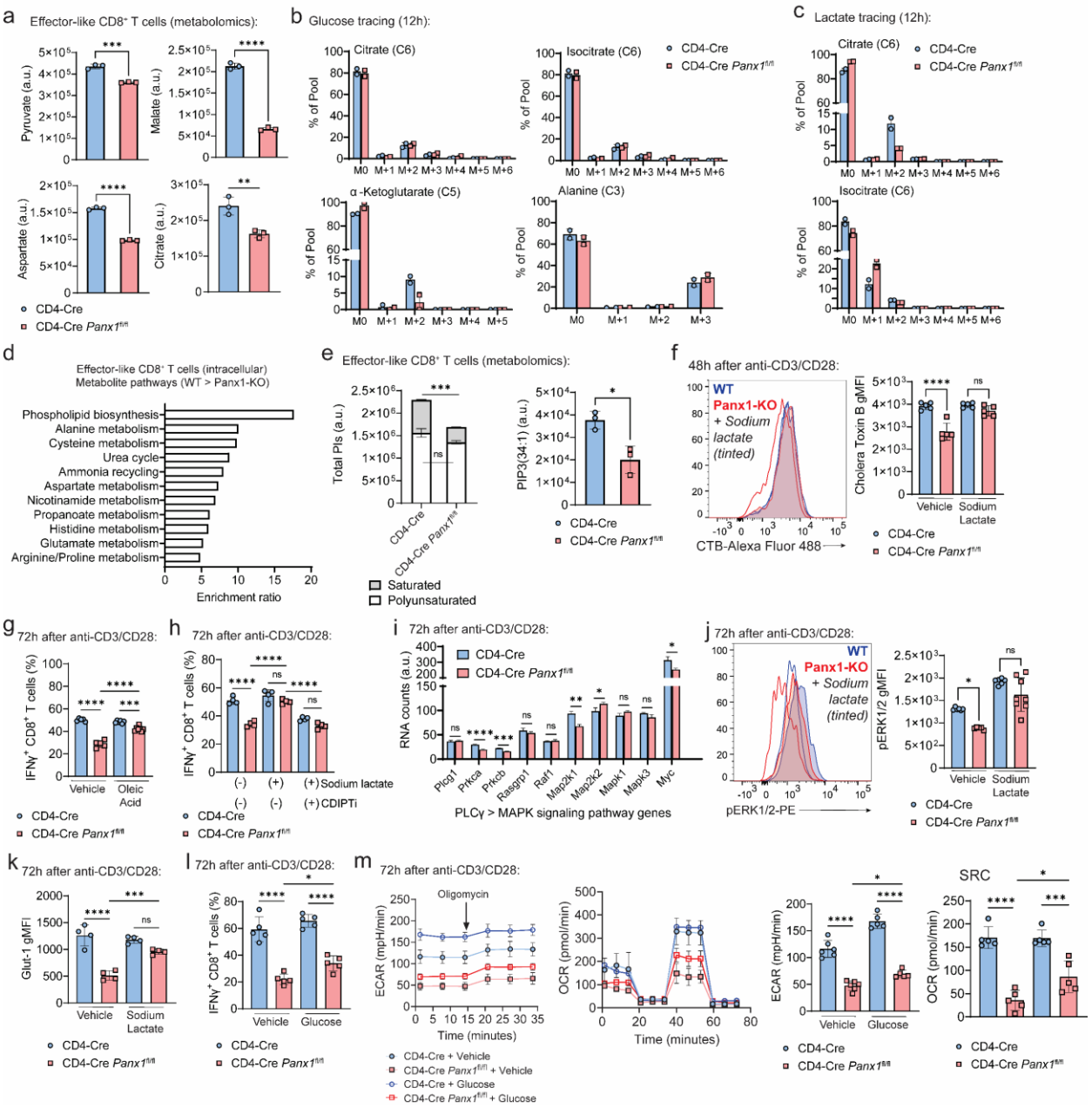


1232

1233 Figure 5

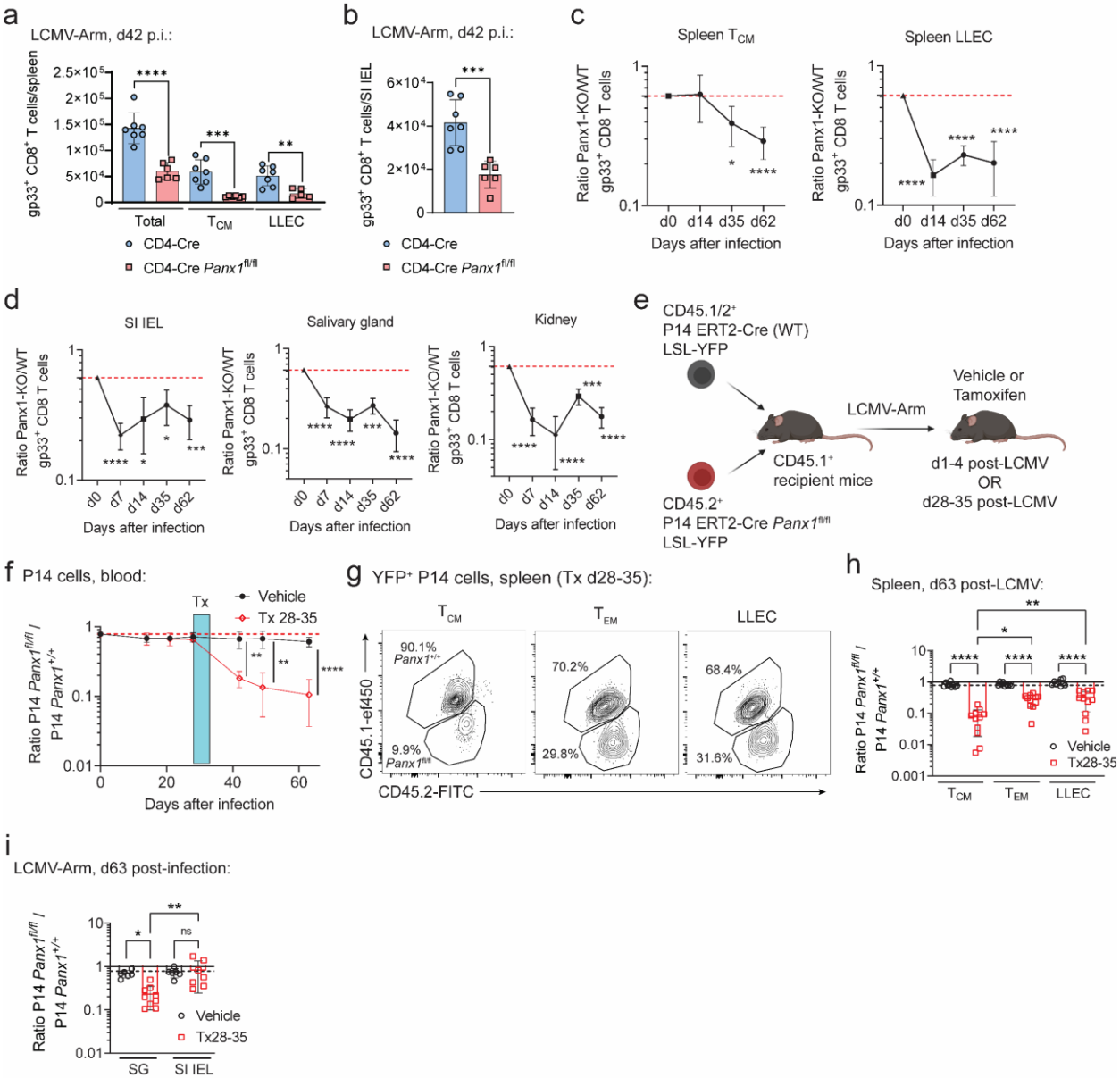


1234
1235

Figure 6

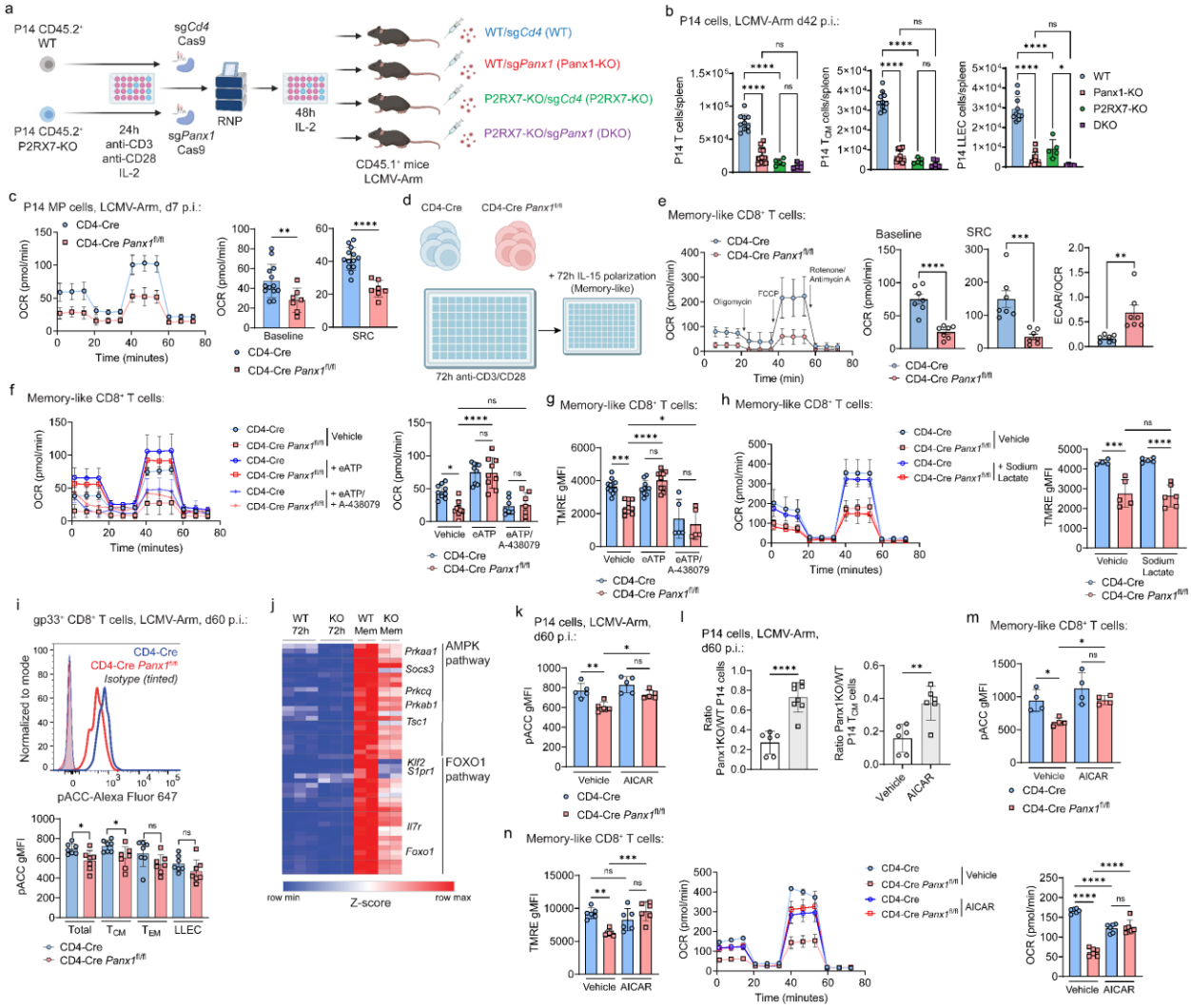
a
P14 CD45.2⁺ WT
P14 CD45.2⁺ P2RX7-KO
sgCd4 Cas9
sgPanx1 Cas9
24h anti-CD3 anti-CD28 IL-2
RNP
48h IL-2
WT/sgCd4 (WT)
WT/sgPanx1 (Panx1-KO)
P2RX7-KO/sgCd4 (P2RX7-KO)
P2RX7-KO/sgPanx1 (DKO)
CD45.1⁺ mice LCMV-Arm
b
P14 cells, LCMV-Arm d42 p.i.:
P14 T cells/spleen
P14 T_CM cells/spleen
P14 LLEC cells/spleen
WT
Panx1-KO
P2RX7-KO
DKO
c
P14 MP cells, LCMV-Arm, d7 p.i.:
CD4-Cre
CD4-Cre Panx1fl/fl
OCR (pmol/min)
Time (minutes)
Baseline
SRC
d
CD4-Cre
CD4-Cre Panx1fl/fl
+ 72h IL-15 polarization (Memory-like)
72h anti-CD3/CD28
e
Memory-like CD8⁺ T cells:
Oligomycin
FCCP
Rotenone/ Antimycin A
Time (min)
ECAR/OCR
f
Memory-like CD8⁺ T cells:
Vehicle
+ eATP
+ eATP/ + A-438079
g
Memory-like CD8⁺ T cells:
TMRE gMFI
h
Memory-like CD8⁺ T cells:
+ Sodium Lactate
Sodium Lactate
i
gp33⁺ CD8⁺ T cells, LCMV-Arm, d60 p.i.:
Isotype (tinted)
Normalized to mode
pACC-Alexa Fluor 647
pACC gMFI
Total
T_CM
T_EM
LLEC
j
WT 72h
KO 72h
WT Mem
KO Mem
Prkaa1
Socs3
Prkcq
Prkab1
Tsc1
Klf2
S1pr1
Il7r
Foxo1
AMPK pathway
FOXO1 pathway
row min
Z-score
row max
k
P14 cells, LCMV-Arm, d60 p.i.:
Vehicle
AICAR
l
P14 cells, LCMV-Arm, d60 p.i.:
Ratio Panx1KO/WT P14 cells
Ratio Panx1KO/WT P14 T_CM cells
m
Memory-like CD8⁺ T cells:
n
Memory-like CD8⁺ T cells:

1239 Figure 7

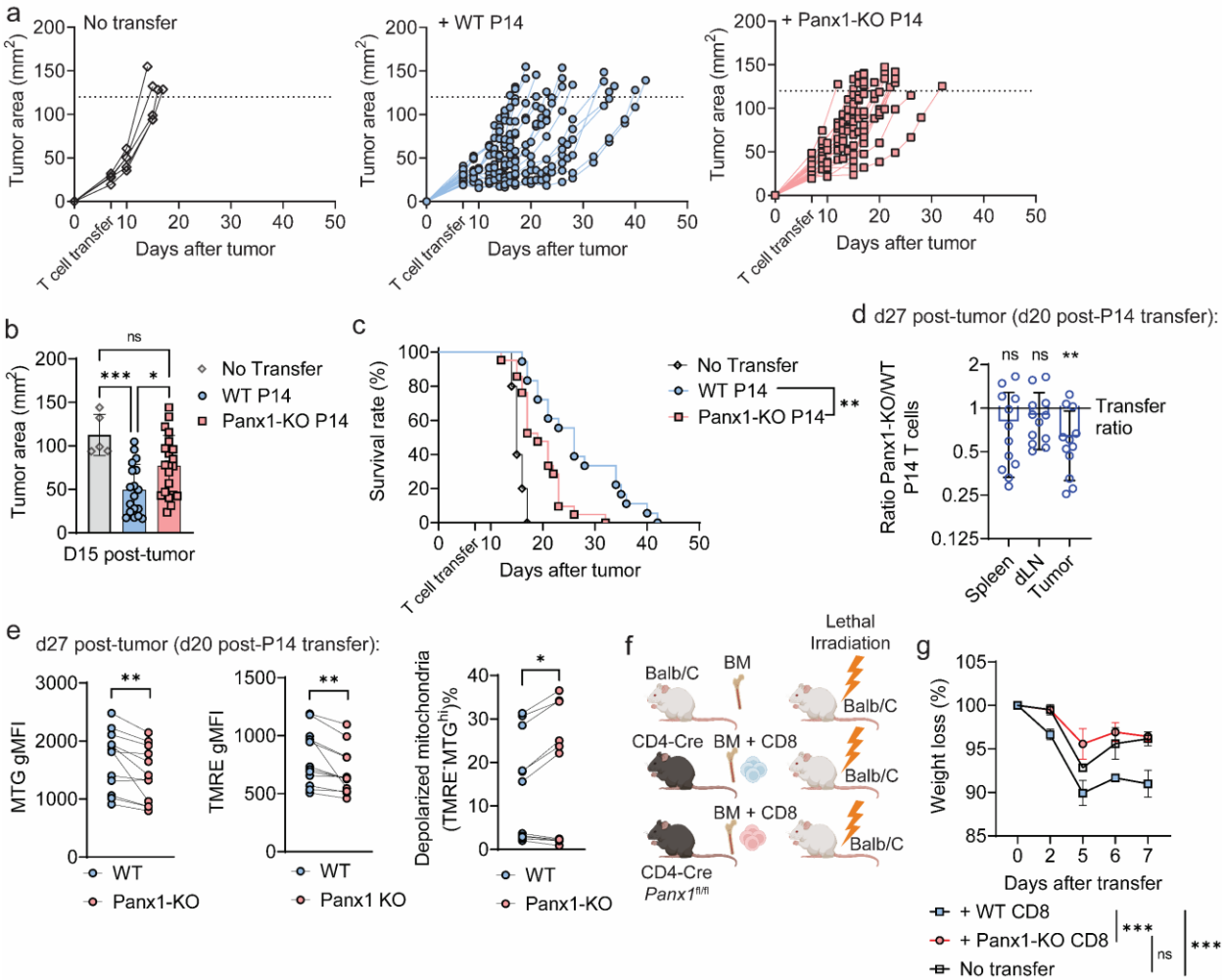


1240